



# **Tectonic termination of oceanic detachment faults, with constraints on tectonic uplift and mass wasting related erosion rates**

Javier Escartín, Barbara John, Mathilde Cannat, Jean-Arthur Olive, Michael Cheadle, Gretchen Früh-Green, Carol Cotterill

## **► To cite this version:**

Javier Escartín, Barbara John, Mathilde Cannat, Jean-Arthur Olive, Michael Cheadle, et al.. Tectonic termination of oceanic detachment faults, with constraints on tectonic uplift and mass wasting related erosion rates. *Earth and Planetary Science Letters*, 2022, 554, 10.1016/j.epsl.2022.117449 . hal-03811932

**HAL Id: hal-03811932**

**<https://cnrs.hal.science/hal-03811932>**

Submitted on 12 Oct 2022

**HAL** is a multi-disciplinary open access archive for the deposit and dissemination of scientific research documents, whether they are published or not. The documents may come from teaching and research institutions in France or abroad, or from public or private research centers.

L'archive ouverte pluridisciplinaire **HAL**, est destinée au dépôt et à la diffusion de documents scientifiques de niveau recherche, publiés ou non, émanant des établissements d'enseignement et de recherche français ou étrangers, des laboratoires publics ou privés.

Revised Feb. 2022

**Tectonic termination of oceanic detachment faults, with constraints  
on tectonic uplift and mass wasting related erosion rates**

*Javier Escartín<sup>1</sup>, Barbara John<sup>2</sup>, Mathilde Cannat<sup>3</sup>, Jean-Arthur Olive<sup>1</sup>,  
Michael Cheadle<sup>2</sup>, Gretchen Früh-Green<sup>4</sup> & Carol Cotterill<sup>5</sup>*

<sup>1</sup>Laboratoire de Géologie – CNRS, UMR 8538, École Normale Supérieure, PSL  
University, Paris, France

<sup>2</sup>Department of Geology & Geophysics, Univ. of Wyoming, Laramie, WY, 82071 USA

<sup>3</sup>Université de Paris, Institut de physique du globe de Paris, CNRS, F-75005 Paris,  
France

<sup>4</sup>Institute of Geochemistry and Petrology, ETH Zurich, Clausiusstrasse 25, 8092  
Zürich, Switzerland

<sup>5</sup>US Science Support Program (USSP), IODP, Columbia University, USA.

**Abstract**

New high-resolution bathymetric data from Atlantis Massif and surrounding seafloor (30°N, Mid-Atlantic Ridge) records avolcanic extension associated with the formation of the axial rift valley floor, following the tectonic truncation of an active corrugated oceanic detachment fault system. The truncated Atlantis detachment is tectonically uplifted by a high-angle valley-bounding normal fault, formed after westward migration of the ridge at ~0.4 to 0.1 Ma. Detachment fault remnants, with preserved corrugations, lie within the present-day rift valley seafloor, and demonstrate that a ~20 km ridge section in the immediate vicinity of the Atlantis Fracture zone has not recorded any recent volcanic activity. Avolcanic extension may thus occur locally at the slow-spreading Mid-Atlantic Ridge, albeit for limited periods of time (less than a few hundred thousand years). The new fault dissecting the detachment shows a throw of ~2800 m, partly due to flexural uplift. Emplacement of the Lost City hydrothermal site occurred at a late stage post-dating the detachment truncation and avolcanic rift valley formation. From the inferred timing of the westward ridge axis shift we calculate uplift rates  $\geq 7$  mm/yr, possibly as high as 33 mm/yr, which are equivalent to or greater than the fastest vertical uplift rates of active normal faults measured to date on Earth (Gulf of Corinth). Geomorphologic observations also demonstrate that mass wasting efficiently reworks the seafloor topography. We obtain local incision and erosion rates  $\geq 1$ -2 mm/yr locally, and as high as 4-8 mm/yr, depending on the assumed age for the rift bounding fault (0.4 vs. 0.1 Ma respectively). Our results suggest that (1) avolcanic extension may occur locally at the slow-spreading Mid-Atlantic Ridge, albeit for limited periods of time (less than a few 100s of kyrs), and (2) document that shifts in axial valley location related to the abrupt abandonment of detachment faults is a first-order process in the asymmetric accretion of slow-spread oceanic lithosphere.

**1. Introduction**

Oceanic lithosphere formed along slow-spreading mid-ocean ridges is shaped by a balance between axial magma supply and tectonic extension. Along ridge sections with limited melt supply, deformation can localize onto a single, large-offset normal fault (detachment). Continued extension exposes lower oceanic crust and mantle at the seafloor along fault surfaces that commonly display extension-parallel corrugations (e.g., Cann et al., 1997; Tucholke et al., 1998; Parnell-Turner et al., 2018), or smooth fault surfaces identified along the ultra-slow SW Indian Ridge (Cannat et al., 2006). In contrast, greater melt supply to the brittle lithosphere promotes magmatic accretion, and formation of limited slip (100s m) normal faults, defining ubiquitous ridge-parallel abyssal hills (Smith et al., 2008; Escartín et al., 2008; Cannat et al., 2009). The transition between these accretion modes is abrupt, not gradual. Numerical models suggest a melt supply threshold, or *M*-value, that describes the ratio between the melt flux supplied to the brittle lithosphere and the total flux required to fully accommodate plate separation (e.g., Buck, 1988; Buck et al., 2005; Tucholke et al., 2008; Olive et al., 2010; Howell et al., 2019). A model threshold of  $M \sim 0.5$  is consistent with the sudden changes in accretion recorded by bathymetry both along-axis (Howell et al., 2019) and across-axis, representing short periods of plate spreading (e.g., Okino et al., 2004; Smith et al., 2006; Cannat et al., 2006; 2009; Escartín et al., 2008).

Widespread exposures of denuded oceanic core complex footwalls on the seafloor form at intermediate to ultra-slow spreading rates (Tucholke et al., 2008), but oceanic detachments have a limited life span from initiation to death of typically  $\sim 1$  Myrs and up to  $\sim 4$  Myrs (Tucholke et al., 1998; John and Cheadle, 2010; Tani et al., 2011; Ohara, 2016). In addition, asymmetric seafloor spreading has been reported associated with oceanic detachments, with  $\sim 60\%$  to  $>85\%$  of the full plate separation accommodated by the active faults (e.g., Searle et al., 2003; Okino et al., 2004; Baines et al., 2008; John and Cheadle, 2010). This asymmetry prompts detachment fault migration towards the ridge axis and adjacent plate, with two possible fates due to lateral ridge shifts or migration (e.g., MacLeod et al., 2009; Cheadle et al., 2012; Reston et al., 2002; Cannat et al., 2009; Cheadle et al., 2019). Firstly, they may be abandoned and rafted off-axis, structurally intact with a well-preserved hanging wall cut off; this is the case of the

Kane detachment at 23°N on the Mid-Atlantic Ridge (MAR) (Dick et al., 2008). Alternatively, the detachment fault can be cut by new high angle faults. The youngest, most recently exposed portion closest to the hanging wall cut off, dismembered from the rest of the detachment fault, may be obliterated by subsequent crustal accretion, including associated faulting and magmatism (e.g., Escartín et al., 2003; Cannat et al., 2009), or be partially preserved on the conjugate flank, as for the MAR 5°S (Reston et al., 2002).

Understanding how detachments are tectonically terminated requires constraints on the timing and rates at which subsequent faulting occurs, as well as assessing potential links to magmatic and tectonic processes on-axis. Tectonic decapitation may also transfer lithospheric remnants from the footwall of the old detachment fault to the footwall of the new fault, as exhibited by flip-flopping and cross-cutting detachments at ultra-slow spreading ridges (Reston, 2018; Sauter et al., 2013). This material transfer across the plate boundary modulates the architecture of the oceanic lithosphere, and is key to unravel associated seafloor magnetic signals.

Atlantis Massif at 30°N on the MAR (Figure 1) is one of the best-studied oceanic core complexes along the global mid-ocean ridge system (Cann et al., 1997; Schoolmeesters et al., 2012; Blackman et al., 2002; Karson et al., 2006; Früh-Green et al., 2018; Grimes et al., 2008). This detachment is adjacent to, and north of, the Atlantis Fracture Zone, that offsets the ridge axis laterally by ~70 km, or ~6 Myrs (e.g., Zervas et al., 1995). Other core complexes are exposed on older seafloor to the west of Atlantis Massif and to the south, at the southern ridge-transform intersection (e.g., Blackman et al., 2008). Recent high-resolution bathymetry (~20m per pixel) acquired during IODP Expedition 357 (Früh-Green et al., 2017) show this detachment system cut by late, ridge-parallel, high-angle normal faults, the most significant of which has a throw that decreases from >2 km in the south, near the ridge-transform intersection, to <500 m at the segment center northwards (Figures 1B, 2, 3; Supplementary Figure S1). The new high-resolution bathymetry, combined with the previous work at Atlantis Massif, makes this area particularly well-suited to study detachment termination through high-angle faulting, and to address several key questions, including a) the mechanisms and timing of

faulting involved in ‘terminating’ oceanic detachment faults, and b) the resulting lithospheric structure and composition (e.g., Reston, 2018).

Here we constrain the chronology of the transition from detachment fault slip to seafloor spreading via rift valley development. We rely on a detailed interpretation of seafloor morphology, combined with existing geologic, geochronologic, and geophysical constraints. We benefit from geophysical surveys (seismic imaging, microseismicity) (Canales et al., 2008; Xu et al., 2009; Collins et al., 2012; Henig et al., 2012), subseafloor sampling from three IODP expeditions (Blackman et al., 2011; Früh-Green et al., 2018), and deep-sea vehicle observations and sampling (Blackman et al., 2002; Karson et al., 2006). IODP Expeditions 304 and 305 drilled several boreholes across the corrugated detachment surface, including the ~1500 m deep hole, U1309D, at the center of the Massif (Blackman et al., 2011). Subsequently, IODP Expedition 357 drilled shallow boreholes (to 15 m below seafloor) along the southern ridge of the core complex, parallel to the spreading direction (Früh-Green et al., 2018). With temporal constraints from thermochronologic studies of samples, as well as geological and geodynamic data, we quantify both uplift and denudation rates.

## **2. Atlantis Massif and its detachment system**

Oceanic detachment systems exposing corrugated fault surfaces exposed at the seafloor were first recognized at the Atlantis Massif along the MAR at 30°N (Cann et al., 1997). This detachment fault formed on the western flank of the Mid-Atlantic Ridge immediately north of the Atlantis Fracture zone (Figure 1). The striated detachment fault surface accommodates >15 km of extension at its southern end, where it is shallowest (~700 mbsf), and underlain dominantly by peridotite intruded by gabbroic rocks outcropping at the transform valley wall (Schroeder and John 2004; Karson et al., 2006). Footwall rocks host the Lost City hydrothermal field, at mass-wasting scarps eroding the detachment (Früh-Green et al., 2003; Kelley et al., 2005), with vent fluid chemistry recording interactions with ultramafic rocks and gabbroic bodies at depth (Proskurowski et al., 2006; Seyfried et al., 2015). To the north, the domal and striated

detachment surface both deepens and its seafloor exposure tapers. Lithologic heterogeneity of the footwall is documented by 1.5 km of gabbroic rocks drilled at IODP borehole U1309D (Ildefonse et al., 2007; Blackman et al., 2011), and supported by a complex three-dimensional seismic velocity structure of the footwall (Canales et al., 2008; Xu et al., 2009; Henig et al., 2012).

Along the northern Atlantis Massif a seismic reflector interpreted as the detachment fault underlies the basaltic hanging wall block, ridgeward of the hanging wall cutoff ( $\sim 30^{\circ}10'N$  to  $\sim 30^{\circ}17'N$ ; Seismic Line MEG-5, Canales et al., 2004), with a  $<15^{\circ}$  eastward dip. Fault curvature is attributed to footwall flexure during extension (Lavie et al., 1999), and requires significant rotations, consistent with paleomagnetic data recording up to  $\sim 50^{\circ}$  anticlockwise rotations away from the ridge axis (Morris et al., 2009); footwall rotations of comparable magnitude are also inferred from bathymetry and paleomagnetic studies at other detachments (Garcés and Gee, 2007; Smith et al., 2008; Schouten et al., 2010; Hansen et al., 2013; MacLeod et al., 2009; Allerton and Tivey, 2001). Hydroacoustic monitoring documents microseismicity within the footwall, along the rift valley walls, and below the ridge valley floor, suggesting a complex pattern of deformation, including strike slip events (Collins et al., 2012).

The spreading half-rate in this area, averaged over the last  $\sim 10$  Myrs, is  $\sim 12$  mm/yr (Zervas et al., 1995; Pariso et al., 1995). Pb-U zircon ages from gabbroic rocks sampled in the footwall over  $\sim 6$ -7 km across the southern ridge parallel to the spreading direction yield a detachment slip rate of  $\sim 28 \pm 6.7$  mm/yr over the last 1.2 Myrs (Grimes et al., 2008). This rate is of the same order as the full spreading rate, and implies significant asymmetry in plate spreading, as proposed for other oceanic detachment faults (Grimes et al., 2011; Searle et al., 2003; Okino et al., 2004; Mallows and Searle, 2012; Fujiwara et al., 2003; Baines et al., 2008). Along the eastern limit of the southern ridge of Atlantis Massif, the detachment is truncated by the high-angle normal fault bounding the western side of the present-day rift valley. To the north, this fault bounds a rafted and uplifted hanging wall block (Figures 1, 3). Late, post-detachment faulting patterns suggest abandonment of the detachment system, with the development of a prominent rift valley, and the off-axis rafting of the inactive, faulted detachment.

### 3. Volcanic features, tectonic structure, and surface processes constrained by seafloor geomorphology

A high-resolution Atlantis Massif bathymetric survey was conducted onboard *RRS James Cook* during IODP Expedition 357 (Früh-Green et al., 2018). These data complement the *MARVEL 2000* survey (Blackman et al., 2002), and other open-access data ([www.gmrt.org](http://www.gmrt.org); Ryan et al., 2009) (Figure 1A). The 20 m resolution grid (Figure 1B) is publicly available (<https://doi.org/10.1594/PANGAEA.935687>), and was analyzed using shaded relief maps (Figure 1B, S1A, S1B), slope maps (Figure S1C), and 3D visualizations (Figures 1C, S2), to map features associated with volcanic, tectonic, and mass-wasting processes (Figures 2, 3), their interactions, and relative timing of formation. Four structural domains are defined, including: A) the Atlantis detachment system (A in Figure 1B); B) the present-day adjacent axial rift valley (RV in Figure 1B); C) seafloor conjugate to the detachment system along the eastern flank of the rift valley (C in Figure 1B); and D) the Atlantis Transform system bounding the detachment to the south (T Figure 1B). We do not interpret older seafloor in the eastern and westernmost regions, nor the full transform valley domain at the edges of the study area.

We map seafloor features related to i) volcanic processes, ii) tectonic processes, and iii) surface processes (Figures 1B, 1C, 2, 3). Each set of features have implications for the cessation of extension along the detachment fault, its truncation by rift-bounding faults, and the feedbacks between volcanic, tectonic and surface processes at slow-spreading MORs.

#### *Seafloor volcanic features*

Volcanic seafloor features include cones, ridges, and hummocky terrain (Figure 3). The present-day rift valley floor (RVF) is limited by the western and eastern rift-bounding faults (WBF and EBF). North of 30°07'N it exhibits volcanic cones, ridges, and



hummocky textured seafloor north, characteristic of volcanically resurfaced ridge axis sections (Smith et al., 1999; Yeo et al., 2011). South of 30°07'N the rift valley seafloor is smooth and lacks volcanic features (Figures 1B, 2C, 3). East of the present-day rift valley a ~10-km-wide strip of volcanic terrain, displaying both seamounts and hummocks, extends the entire segment length to the Atlantis Fracture Zone. This terrain corresponds to the paleo-rift valley floor (PRVF; Figure 3), and records a capture of the valley floor by the African plate via a westward axis jump.

On the western flank of the present-day rift valley, volcanic seafloor is restricted to the area between the hanging wall cut off and WBF (Figure 3). This terrain corresponds to hanging wall blocks rafted above the east-dipping detachment fault. Fresh volcanic deposits (glass/hyaloclastite) have also been identified above the detachment locally (*v* in Figure 3; Früh-Green et al., 2018), in an area lacking corrugations and with irregular surface, also lacking clear volcanic structures (Figures 1B, 3).

#### *Tectonic features.*

Tectonic features across the area record a protracted history of faulting. The most prominent are ridge-parallel normal faults which extend along-axis for hundreds of m to >30 km (WBF and EBF, Figure 3). The vertical throw of these faults varies both among them and along their strike, locally exceeding 2 km on the southern end of the WBF that dissects the Atlantis detachment fault (Figure 3). The Atlantis Fracture Zone and associated transform valley show numerous rectilinear, subparallel scarps and ridges related transform tectonics.

Figure 3 highlights the well-preserved corrugated fault surface exposed at the seafloor of the Atlantis detachment fault system (ADS), and the hanging-wall cutoff, preserved along the northern part of the ADS. In contrast, the footwall cutoff is poorly defined, with several positions proposed (Canales et al., 2004; Schoolmeesters et al., 2012); this system lacks prominent ridges with back-tilted volcanic seafloor commonly observed

at the footwall cutoff along several MAR detachments (Smith et al., 2008; Escartín et al., 2017).

We identify three potential footwall cutoff positions (FWC in Figure 3), one oblique to the axis following the eastern limit of the corrugated surface, and two axis-parallel ones from prior studies (Canales et al., 2004). Hanging-wall cutoffs are used in conjunction with geochronologic constraints (Grimes et al, 2008; Schoolmeesters et al, 2012) to obtain a range of plausible total tectonic extensions, associated ages, and timing and rate of spreading accommodated by the detachment.

Minor faults that are recent and may be linked to the recorded seismicity in the area (e.g., Collins et al., 2012) dissect the exposed corrugated detachment surface, displaying jagged and irregular traces, and associated small vertical throws (<5 m). These are not resolvable in shipboard bathymetry, visible only as subtle slope breaks (Figures 2A, 2B, 3). The detachment surface is not clearly identifiable at its southwestern corner, that displays complex seafloor texture that has yielded volcanic rocks (*v* in Figure 3), suggesting late volcanism and lava emplacement on the detachment surface.

Figure 3 shows two sections of seafloor interpreted as preserved corrugated detachment fault surface fragments, both along the fault scarp dissecting the detachment, and at the rift valley floor (*cds*, Figure 2C). These detachment remnants are identified based on lateral continuity of corrugations (Figures 2, 3), from the uplifted, shallowest detachment fault surface, to the rift valley floor, over flowline-parallel distances of >15 km. This continuity is confirmed by axis-parallel profiles over the detachment and these remnants, showing that both the vertical amplitude and lateral spacing (along-axis) of the corrugations are consistent (Figure 4). These corrugated fault remnants are thus reliable tectonic markers to determine vertical fault displacements.

*Surface process features*

The new high-resolution bathymetry reveals numerous features associated with surface (seafloor) processes. Both the nodal basin at the end of the ridge axis adjacent to the Atlantis Fracture Zone, and zones along the transform valley, are flat-bottomed sediment ponds ( 'N' in Figure 1; 'sp' in Figure 2C and slope map, Figure 2D). Sediments in the nodal basin partially cover the southern part of the detachment fault remnant at the rift valley floor (Figure 4B).

Mass wasting is pervasive throughout the study area. Prominent, large headwall scarps (up to several km across) are visible along the southern wall of Atlantis Massif towards the transform valley, and along the southern WBF scarp, where it is highest. This mass wasting has significantly eroded the massif, exposing footwall rocks in the upper scarp amphitheaters, and along erosional gullies down-slope. Figure 4C highlights up to 2 km northward retreat of the scarp forming the southern wall of Atlantis Massif. The scar bases often display slump and pressure ridges common at gravity-driven mass-wasted deposits. Smaller head scarps also occur over the corrugated detachment, including areas with very low topographic gradients and vertical relief.

We identify several incipient head-wall scarps recording active mass wasting of the detachment. A curved, semi-circular incipient scarp, similar to larger headwall scarps on the southern side of the massif, is centered at 30°10'N. With a diameter of ~5 km and a height <10 m, it cuts the corrugated detachment, the hanging wall cutoff, and uplifted hanging wall block to the east (Figure 3). Upon collapse, this structure may preserve a down-dropped detachment remnant, as observed along the western rift valley wall.

#### 4. Age constraints

To quantify the rates of deformation, tectonic uplift, and ultimately those related to surface processes (e.g., scarp erosion due to mass wasting) we require temporal constraints on the tectonic evolution of Atlantis Massif. We focus on a) estimating the age of the footwall cutoff formation, corresponding to detachment

initiation, b) determining the duration of slip along the detachment, and c) timing the detachment truncation by rift bounding wall, associated with a westward shift of the ridge. These time constraints are based on spreading age, calculated from distances to the axis and assumed spreading rates, and from geochronologic constraints, including Pb-U and (U/Th)He zircon dates (Grimes et al, 2008; Schoolmeesters et al, 2012). With these, we seek to provide plausible age ranges for each of the major features defining the tectonic history of the Atlantis Massif.

Regional surface magnetic anomalies yield a full spreading rate of  $\sim 23$  mm/yr, and a modest asymmetry since anomaly 2A ( $\sim 3$  Ma), with 12 mm/y to the West and 11 mm/yr to the East (Zervas et al., 1991). A present-day full rate of 23.6 mm/yr is predicted by the NUVEL-1 model (Argus and Gordon, 1991), while later regional magnetic study (Pariso et al., 1995) yields a full spreading rate of 24 mm/yr. U/Pb zircon geochronology independently constraints slip rates along the Atlantis detachment fault, with values of  $\sim 28 \pm 6.7$  mm/yr over the last 1.2 Myrs (Grimes et al., 2008). More recent estimates by Grimes et al (2011) suggest a lower slip rate of 20 mm/yr. Here we adopt end member spreading rates of 12 and 24 mm/yr to bracket the maximum and minimum ages of tectonic features and events. As shown in Figure 4a, we define a ‘zero age crust’ at the eastern limit of the detachment fault surface remnant, located in the middle of the rift valley along Profile A-A’. This spreading-parallel profile crosses the Atlantis detachment system where it is best developed, recording the full history of detachment formation and subsequent evolution.

*Footwall cutoff (breakaway) age.* Lacking a clear footwall cutoff ridge common at many oceanic detachments (e.g., 13,20’N, Escartín et al., 2017), Figure 4 shows two possible footwall cutoffs, at 20 (FC2 in Figures 4a, 4c) to 24 km (FC1) away from the ridge axis, as interpreted from this and prior studies (e.g., Canales et al., 2004). Assuming a regional spreading half-rate of 12 mm/yr, the footwall cutoff age would be  $\sim 1.7$  to  $\sim 2$  Ma. However, if we assume the detachment fault slipped at the end-member full spreading rate of 24 mm/yr inferred from U/Pb zircon geochronology (Grimes et al, 2011), then we have to remove the extension that occurred after the detachment fault ceased to slip. The detachment is truncated by the WBF, vertically offsetting the

detachment fault by at least ~2.8 km. Hence, the horizontal distances reported above include the tectonic extension associated with WBF, and the actual spreading distance should be reduced by ~1.7 km (assuming an initial fault dip of ~60°), to ~18.3 and 22.3 km, respectively. We thus obtain footwall cutoff ages of 0.76-0.92 Ma. Together, these two end-member calculations yield minimum and maximum footwall cutoff ages of ~2 and ~0.8 Ma. However, gabbroic rocks in the Atlantis Massif footwall have Pb/U zircon dates of ~1.2 Ma (Grimes et al., 2008), further restricting this time interval, as the detachment is required to develop in lithosphere of this age or older. We thus estimate the age of the detachment footwall cutoff between ~2 and 1.2 Ma.

#### *Duration of detachment fault slip.*

As discussed, the two possible footwall cutoffs lie at 20 to 24 km west from the ridge axis (Figure 4A). Later tectonic extension associated with the WBF accounts ~1.7 km of this distance, and so reduces the slip on the detachment to ~18.3 and 22.3 km, respectively. End-member half-spreading rates of 24 and 12 mm/yr (see above) yield detachment fault slip durations ranging from ~0.8 to ~1.9 Ma. An average slip-rate of 20 mm/yr (Schoolmeesters et al., 2012) would yield slip durations between 0.9 to 1.1 Ma.

*Detachment truncation of by rift valley bounding fault.* The truncation must post-date the age of the plutonic rocks on the footwall, which were sampled to 1.5 km below seafloor (IODP Hole U1309D), and along the south wall of Atlantis Massif in HOV Alvin dives (Karson et al., 2006). The youngest Pb-U zircon date for the gabbro solidus of 800°-850°C is ~1.0 Ma (Grimes et al., 2008). Based on the distribution of cooling temperatures within borehole U1309D, Schoolmeesters et al. (2012) proposed that the detachment fault stopped operating at ~0.4 Ma. These age constraints suggest that the rift-bounding fault truncated the detachment within the last 400,000 years, post-dating the youngest age provided by geo- and thermochronology of footwall rocks.

## **5. Discussion**

### *5.1. Avolcanic rift valley formation*

Our observations demonstrate that since formation of the present-day rift valley (<0.4 Ma), no volcanic activity occurred along the 20 km of ridge axis adjacent to the Atlantis Fracture Zone (Figure 3). At the southern end, a flat-bottomed, sedimented nodal basin developed within ~10 km of the Atlantis Transform Fault, with a seafloor depth of 4950 m. The nodal basin transitions north to a detachment remnant paving the axial valley floor, extending ~10 km along-axis, and with corrugations matching those of the main, uplifted detachment fault surface westwards. This remnant lies ~600-700 m above the nodal basin floor (bathymetric Profile F, Figures 4b, 4c).

Stacked bathymetric profiles (Figure 4b) also indicate plausible nodal basin infill thickness. Five along-axis profiles across Atlantis Massif are shifted vertically to align the shallowest parts of the dome-shaped detachment surface. Mass-wasting along the transform wall, with associated head scarps, erodes the detachment surface northwards. Profile D samples a significant length of the detachment surface preserved from mass-wasting, along an apron extending southwards. Assuming that the along-axis detachment shape in profile D is preserved during the life-span of the detachment, the relative relief differences between profiles F and D at the nodal basin thus provides an estimate of the maximum sediment thickness, likely exceeding 1 km locally (Figure 4b).

The transition between volcanic and avolcanic rift valley floor is abrupt at ~30 °07'N; stacked profiles suggest that at distances >12 km North of the transform fault any young remnant of the detachment is disrupted or resurfaced by recent volcanism. Avolcanic seafloor has been reported along the ultra-slow spreading South West Indian ridge (e.g., “nearly amagmatic seafloor”, Cannat et al., 2019), associated with detachment faults operating on-axis; this is a type of seafloor as yet described or identified to date however at slow-spreading ridges. The lack of volcanism along the rift valley near the Atlantis Transform is plausibly due to cooling by the juxtaposition of cold, 6-Myr-old lithosphere across the Atlantis transform. Possible cooling-related mechanisms include efficient suppression of melt production at depth, efficient entrapment of melt within a lithosphere that thickens towards the transform, or a combination of both.

366

367 *5.2. Recent rift valley formation and detachment truncation*

368 Initiation of the detachment ~1.2 to 2 Myrs ago created a hanging wall cutoff that  
 369 extends ~27-30 km along-axis, corresponding to the maximum along-axis length of the  
 370 corrugated surface, and the preserved ridges interpreted as potential footwall cutoff  
 371 remnants (Figures 3, 5a). The detachment fault tapered to the north, accommodating  
 372 extension only along ~15 km of ridge axis adjacent to the transform fault (Figures 5b,  
 373 c). The terrain formed north of the active detachment surface displays seafloor  
 374 textures typical of volcanic terrains, with identifiable volcanic cones, and small offset  
 375 normal faults. This suggests that the threshold in magma emplacement in the shallow  
 376 crust migrated, corresponding to the transition from volcanic to avolcanic plate  
 377 spreading. This volcanic off-axis terrain is dissected by the WBF that continuously  
 378 extends southward towards the transform fault, also dissecting the detachment fault  
 379 surface (Figure 5d).

380 The present-day axial valley is bound to the west by the steep fault that truncated the  
 381 detachment as the axis shifted westward (Figure 5e), with several consequences. In the  
 382 northern part of our study area, the extent of volcanic seafloor on either side of the  
 383 present-day rift valley is asymmetric about the present-day axis (Figure 3), suggesting  
 384 that the new axial graben developed along the western edge of the earlier one, possibly  
 385 exploiting the associated rift-bounding walls. This lateral shift also preserved and  
 386 displaced a mostly unfaulted, ~10 km wide strip of seafloor eastwards (PRVF, Figure  
 387 3), a width that is typical of rift valleys along many slow-spreading ridge sections (e.g.,  
 388 Thibaud et al., 1998). The maximum vertical throw of the WBF scarp is ~2800 m,  
 389 between the eastern edge of the corrugated surface to the west, and the depth of the  
 390 lowermost detachment remnant paving the rift valley (Figure 4a). WBF tapers  
 391 northwards to ~1 km over ~10 km along-axis. Based on this tectonic configuration and  
 392 history, the former hanging-wall cutoff (or “termination”), neither preserved nor  
 393 recognizable in the bathymetry, must be east of the detachment remnant at the rift  
 394 valley. We speculate that the former hanging wall cutoff is truncated by the EBF fault  
 395 (Figure 3), or covered by debris from this fault at its base. The Lost City hydrothermal

field, that records fluid flow over the last ~30 kyrs (e.g., Fruh-Green et al., 2003) was emplaced following the formation of the rift valley, and at the southern end of the tectonically uplifted and eroded detachment fault surface (Figures 3, 5).

Bathymetric maps also highlight that spreading-parallel corrugations found on both the main detachment surface (dome at Atlantis Massif) and its remnants to the east are laterally continuous. Figure 4B shows the along-axis bathymetry profiles stacked along a flow line (line A-A', Figure 4c), at the depth of the shallowest corrugations (see Figure 4c, showing profile locations). The detachment surface shape is very similar on profiles B through D (distances from -2 to 10 km in Figure 4b), and the Meg-5 seismic reflection profile (Canales et al., 2004) shows the detachment fault lies beneath uplifted volcanic seafloor along the northern section of Atlantis Massif. The stacked profiles C and D (Figures 4b, 4c) are reference profiles sampling longer along-axis detachment surface sections that are well-preserved. The remaining profiles detail shorter, along-axis detachment sections, and differences in depth relative to the two reference profiles provide first-order constraints on the processes either covering or eroding the detachment. To the North, stacked profiles E and F are progressively shallower and document the volcanic infill of the rift valley floor, with an inferred thickness of volcanic material gradually increasing to >1 km (red shading, Figure 4b). Towards the South, these profiles are also shallow, and depth differences document instead rift valley infill towards the transform (nodal basin, *N* in Figures 1b-c) by both sediment and rubble from mass-wasting from the rift valley and transform walls, and with an infill thickness likely >1 km (green shade, Figure 4b). In contrast, profile B is deeper than reference profiles along the Atlantis Massif southern wall, recording incisions of a few hundreds of m, locally up to ~1 km (yellow shading, Figure 4b).

Prior studies documented faulting and decapitation of corrugated detachment faults by higher-angle normal faults, with the development of high relief scarps (typically ~1 km, up to ~2 km in vertical displacement), both along the Mid-Atlantic Ridge (e.g., Reston et al., 2002; Escartín et al., 2003; Reston, 2018) and the Southwest Indian Ridge (Cannat et al., 2009). Extreme relief across steep, late faults has been interpreted as flexural response of strong lithosphere, as footwall rollover of oceanic detachments is



attributed to flexure of a weak lithosphere (e.g., Schouten et al., 2010). Detachment-terminating scarps have thus been interpreted to result from strengthening of the oceanic lithosphere over a short period of time (~100 kyrs or less), in the absence of pervasive weakening of the footwall by brittle damage, alteration-induced footwall weakening, or both (Cannat et al. 2009). The development of a large-throw (~2.8 km), high-angle fault across Atlantis Massif core complex is compatible with a low effective elastic thickness lithosphere. This is because in the “rolling hinge” model, significant rotation of the exposed detachment surface begins when the horizontal offset on the detachment exceeds ~3 times the (effective) elastic lithospheric thickness (Schouten et al., 2010; Olive et al., 2019). The shape of the escarpment created by a short-offset (< 5 km) normal fault is thus weakly sensitive to effective elastic thickness. Consequently, detachment-terminating faults may well nucleate from one of many areas of weakness developed in the footwall.

Understanding where and how such weak zones form requires a theoretical framework beyond thin plate flexure, owing to the large strains and complex deformation styles involved in footwall exhumation. Sandiford et al. (2021) argue that core complex growth involves primarily solid-body rotation near the active fault, and lithosphere unbending outboard of the hanging-wall cutoff. Most footwall damage and subsequent weakening occurs near the footwall cutoff (breakaway ridge) due to a flexural-isostatic response during initial footwall stages of extension. As extension proceeds, unbending promotes upper lithosphere compression and lower lithosphere extension, forming either antithetic or synthetic faults (e.g., Olive et al., 2016; Sandiford et al., 2021) that may dissect the core complex, a process named footwall snapping by Lavier et al. (2000). Sandiford et al.’s (2021) model also predicts the development of a fault cutting the detachment footwall but with a dip opposite to that of the WBF at Atlantis Massif. Footwall truncation there may have involved external forcing or 3-D effects not captured in 2-D models of core complex formation, such as along-axis rift fault propagation.

### *5.3. Implications for lithospheric structure and composition*

Detachment truncation has implications for the structure and composition of the oceanic lithosphere, and for its tectonic history. Detachment decapitation requires lateral jumps of the ridge axis, possibly transferring sections of the oceanic lithosphere from one flank of the axis to the other. In the case of the Atlantis detachment, the detachment fault within the lithosphere likely underlies the volcanic terrain paving the East flank of the ridge (PVRF, Figures 3, 5e, 5f). This transfer of lithosphere across plates may be favored by asymmetric spreading associated with detachments, typically accommodating >50% of the total plate separation. This process thus requires either a migration of the detachment towards and across the ridge axis (Figures 5b-5d), a jump of the ridge axis into the detachment (Figure 5E), or both, with ridge offsets growing when detachments develop next to symmetrically spreading ridge sections (Howell et al., 2019).

It has been postulated that detachment and ridge axis migration results in the detachment termination due to magmatic emplacement within the footwall, associated with the lateral propagation of adjacent ridge sections (e.g., MacLeod et al., 2009). Our results from Atlantis Massif illustrate tectonic truncation instead, associated with propagation of the faults bounding the adjacent rift valley, in the absence of volcanic activity at the rift floor. The history of detachment truncation has two main implications. First, detachment-bearing seafloor often displays faulted footwalls (e.g., Escartín et al., 2003; Smith et al., 2006; Cannat et al., 2009). As a result, the composition of the lithosphere and its structure will be complex, inheriting sections transferred from one plate to another. This configuration, in the case of extreme extension at ultra-slow spreading segments, has been invoked for the development of flip-flopping detachment faults (e.g., Sauter et al., 2013; Reston, 2018). Second, the detailed tectonic evolution of truncated detachment may strongly modulate seafloor magnetic data, particularly those from high-resolution, near-bottom surveys. Lateral rift shifts capturing lithospheric sections in conjugate flanks will result in a seafloor with a complex and discontinuous accretion history, direction, and age at short timescales.

#### *5.4. Normal fault tectonic uplift rates*

With the bathymetry data, geomorphologic interpretations, and age constraints discussed, we quantify long-term tectonic uplift rates associated with the WBF truncating the detachment, and evaluate possible variations in these rates at geologically short time-scales ( $<1$  Ma). With a maximum vertical throw of 2800 m, and a truncation age of  $\leq 0.4$  Ma, WBF's minimum uplift rate is  $\sim 7$  mm/yr. Assuming a fault dipping between  $\sim 60^\circ$  and  $45^\circ$ , the minimum horizontal slip rates range from  $\sim 4.0$  to 7 mm/yr, with minimum dip-slip rates of  $\sim 8$ -10 mm/yr. These horizontal extension rates, accommodated along a single fault, represent  $\sim 15$ -30% of the present-day full spreading rate. These tectonic rates may be significantly faster if the rift-bounding fault is younger than the maximum age of 0.4 Ma inferred from footwall rock ages.

In absolute terms, the time-averaged tectonic uplift rate we calculate is probably one of the fastest recorded for any active high-angle fault on Earth, and the first inferred for an active submarine fault. Dip-slip rates of 8-10 mm/yr are comparable to those reported for one of the fastest-slipping low-angle normal faults on-land of  $\sim 12$  mm/yr (Mai'iu fault in Papua New Guinea; Webber et al., 2018). These rates also compare to fast-slipping, steep continental normal faults: based on uplifted marine terraces, De Martini et al, (2004) calculate uplift rates of 7-11 mm/yr along the Aigion and Helike normal faults bounding the Western Gulf of Corinth basin, with total extension rates of  $\sim 16$  mm/yr (Avallone et al., 2004).

There are significant variations in the accommodation of plate separation and associated strain both on short geologic time-scales ( $<500$  ka?), and along axis. Along the southern part of the ridge segment, where corrugated detachment remnants are preserved at an avolcanic rift valley floor, we assume that the extension we document in bathymetry corresponds to that accommodated by the WBF and EBF faults, with throws of  $\sim 2800$  m and  $\sim 750$  m respectively. If these two faults formed at the same time ( $\sim 0.4$  Ma or earlier) and during the westward ridge axis shift, the total horizontal extension that these faults likely accommodate is  $\sim 2000$ -3500 m for fault dips of  $60^\circ$  and  $45^\circ$ , respectively. Lacking volcanic repaving of the seafloor, and assuming an end-member mode of avolcanic extension since the rift valley formation, this corresponds

to ~83,000-150,000 yrs of extension for a full spreading rate of 24 mm/yr. Hence, formation of the present-day rift valley may be significantly younger than the maximum of ~0.4 Myrs for the westward ridge shift. In this end-member avolcanic scenario, the WBF's uplift rates would increase to at least 18-33 mm/yr, with dip-slip rates of up to 25-47 mm/yr or 21-38 mm/yr for 45° and 60° fault dips respectively; these slip rates would be significantly faster than any other normal fault documented on Earth to date. The associated horizontal extension rates (10-19 mm/yr) would imply that >40% of the plate separation (~24 mm/yr) is accommodated tectonically along this WBF.

Avolcanic extension is consistent with the above tectonic strain partitioning, accommodated both by bounding rift fault motion, and by distributed strain throughout the rift valley floor (e.g., fissures, small-scale faulting, or blind diking not breaching the seafloor). However, distributed strain is likely limited, as the detachment fault remnant is well-preserved, and no late-stage faults dissecting its corrugations are observed, as at the uplifted detachment surface to the west (Figures 2A, 2C, 3). Consequently, the rift valley formed earlier than ~0.4 Myrs, and not later than ~0.1 kyrs, with tectonic uplift rates on the WBF likely between a minimum of 7 mm/yr and an absolute maximum of 33 mm/yr. Finally, the volcanically repaved seafloor to the north of the study area suggests a significant melt supply gradient that likely induces along-axis variations of magmatic and tectonic strain partitioning, controlling avolcanic rift formation.

### 5.5. Mass wasting erosion rates

Mass wasting is pervasive and a significant process reshaping transform valley walls and their associated bounding scarps, in addition to ubiquitous abyssal hills (Karson et al., 2006; Cannat et al., 2013). To date we lack adequate quantification of the associated erosion rates, and on the corresponding mass fluxes of debris transported downslope, critical parameters to develop quantitative models of submarine erosion and landscape evolution

Mass wasting is clearly visible throughout the study area (Figure 3), with stacked profiles in Figure 4b revealing incision and erosion along the transform fault wall (Karson et al., 2006). Locally, the incision of the WBF scarp reaches 900 m, with an average of ~450 m (Figure 4). These values suggest that long-term erosion rates associated with mass wasting along steep scarps may be typically ~1 mm/yr, and up to ~2 mm/yr assuming the WBF initiated 0.4 Ma. These rates would increase to values of ~4 mm/yr, and a maximum of 8 mm/yr, if the WBF initiated at 0.1 Ma as outlined above. These values are consistent with geologic observations along the walls of rift-bounding faults, where mass wasting is widely documented both by slump scarps and associated deposits, responsible for a footwall cutoff, retreat and by typical bounding fault scarp angles of ~30° (e.g., Cannat et al., 2013; Escartín et al., 2017; Olive et al., 2019). This scarp morphology indicates that rift-bounding faults, with fault dips of ~60° to ~45°, may be efficiently eroded as they emerge and develop on-axis if the local erosion rates are as high as those inferred here.

## 6. Conclusions

New high-resolution shipboard bathymetric data acquired over the Atlantis Massif detachment system (30°N, Mid-Atlantic Ridge) provides insights into the tectonic termination of detachment faults, and its connections to volcanic processes on-axis. We also quantify rates of both tectonic uplift, and erosion due to mass wasting. The Atlantis Massif detachment system is truncated by a high-angle normal fault reaching ~2.8 km in vertical displacement, partly owing to the flexural lithospheric response. This western rift fault now bounds the present-day rift valley that formed following a westward ridge shift that has preserved the paleo-rift valley seafloor on the East flank of the ridge axis. Remnants of the corrugated detachment fault surface preserved at the rift valley floor unequivocally demonstrate that this tectonic decapitation of the detachment is linked to avolcanic extension along the ridge axis adjacent to the Atlantis transform fault, and that the seafloor is reshaped by volcanism at distances >20 km from the transform fault. Avolcanic extension may thus occur at

slow-spreading ridges, albeit for limited periods of time (less than a few hundreds of thousands of years).

The rift-bounding fault dissecting the Atlantis detachment system formed less than 400,000 years ago, and possibly within the last ~100,000 yrs. This implies minimum vertical uplift rates greater than 7mm/yr, and that may exceed ~30mm/yr, corresponding to the fastest rates reported in a terrestrial environment on Earth. The bathymetry also reveals significant mass wasting along the flanks of the uplifted Atlantis Massif, on the rift valley bounding faults (degrading the normal fault scarp), and in the Atlantis transform valley. Bathymetric profiles indicate incisions that locally exceed 900m, corresponding to erosion rates between ~1 mm/yr and 8 mm/yr for WBF formation, and assuming ages of 0.4 and 0.1 Myrs, respectively. These high erosion rates are also consistent with the low-angle of the rift bounding fault scarp (~30° or less) suggesting efficient erosion coeval with tectonic uplift, and that this efficient erosion is widespread and operates along all slow- and ultra-slow spreading ridges.

**Acknowledgements.** We thank the captain, officers, and crew of aboard RRS James Cook for facilitating sea operations and data acquisition. ESO staff, with their effort and support throughout the duration of this project, supported data gathering and subsequent processing. Processed bathymetry used in this study is publicly available at <https://doi.org/10.1594/PANGAEA.935687>. The Science Party and the PIs contributed to define and support this project. Support was provided by ECORD and IODP France to JE and MC, and by U.S. Science Support Program (SSSP) to BJ. GFG acknowledges funding by the Swiss National Science Foundation (SNF) and subawards from the Deep Carbon Observatory. We acknowledge N. W. Hayman and an anonymous reviewer for comments and suggestions on the manuscript, and editorial handling by J.-P. Avouac.

## References

- Allerton, S., and Tivey, M.A., 2001, Magnetic polarity structure of the lower oceanic crust: *Geophysical Research Letters*, v. 28, no. 3, p. 423–426.
- Argus, D.F., and Gordon, D.G., 1991, No-net rotation model of current plate velocities incorporating plate motion model NUVEL-1: *Geophysical Research Letters*, v. 18, no. 11, p. 2039–2042.
- Avallone, A., Briole, P., Agatza-Balodimou, A.M., Billiris, H., Charade, O., Mitsakaki, C., Nercessian, A., Papazissi, K., Paradissis, D., and Veis, G., 2004, Analysis of eleven years of deformation measured by GPS in the Corinth Rift Laboratory area: *Comptes Rendus Geoscience*, v. 336, no. 4–5, p. 301–311, doi:10.1016/j.crte.2003.12.007.
- Blackman, D.K., Ildefonse, B., John, B.E., Ohara, Y., and D. J. Miller, N. Abe, M. Abratis, E. S. Andal, M. Andreani, S. Awaji, J. S. Beard, D. Brunelli, A. B. Charney, D. M. Christie, J. Collins, A. G. Delacour, H. Delius, M. Drouin, F. Einaudi, J. Escartín, B. R. F. D.K., 2011, Drilling constraints on lithospheric accretion and evolution at Atlantis Massif, Mid-Atlantic Ridge 30°N: *Journal of Geophysical Research*, v. 116, p. B07103, doi:10.1029/2010JB007931.
- Blackman, D.K., Karson, J.A., Kelley, D.S., Cann, J.R., Früh-Green, G., Gee, J.S., Hurst, S.D., John, B.E., Morgan, J., Nooner, S.L., Ross, D.K., Schroeder, T.J., and Williams, E.A., 2002, Geology of the Atlantis Massif (Mid-Atlantic Ridge, 30°N): Implications for the Evolution of an ultramafic oceanic core complex: *Marine Geophysical Researches*, v. 23, p. 443–469.
- Buck, W.R., 1988, Flexural rotation of normal faults: *Tectonics*, 77,959–973, doi:10.1029/TC007i005p00959.
- Buck, W.R., Lavier, L.L., and Poliakov, A.N.B., 2005, Modes of faulting at mid-ocean ridges: *Nature*, v. 434, p. 719–723.
- Canales, J.P., Tucholke, B.E., and Collins, J.A., 2004, Seismic reflection imaging of an oceanic detachment fault: Atlantis megamullion (Mid-Atlantic Ridge, 30°10'N): *Earth and Planetary Science Letters*, v. 222, p. 543–560.
- Canales, J.P., Tucholke, B.E., Xu, M., Collins, J.A., and Dubois, D.L., 2008, Seismic evidence for large-scale compositional heterogeneity of oceanic core complexes: *Geochemistry, Geophysics, Geosystems*, v. 9, no. 8, p. Q08002, doi:10.1029/2008GC002009.
- Cann, J.R., Blackman, D.K., Smith, D.K., McAllister, E., Janssen, B., Mello, S., Avgerinos, E., Pascoe, A.R., and Escartín, J., 1997, Corrugated slip surfaces formed at North Atlantic ridge-transform intersections: *Nature*, v. 385, p. 329–332.
- Cannat, M., Sauter, D., Escartín, J., Lavier, L., and Picazo, S., 2009, Oceanic corrugated surfaces and the strength of the axial lithosphere at slow spreading ridges: *Earth and Planetary Science Letters*, v. 288, p. 174–183.

- 640 Cannat, M., Sauter, D., Mendel, V., Ruellan, E., Okino, K., Escartín, J., Combier, V., and  
641 Baala, M., 2006, Modes of seafloor generation at a melt-poor ultraslow-spreading  
642 ridge: *Geology*, v. 34, no. 7, p. 605–608.
- 643 Cannat, M., Mangeney, A., Ondreas, H., Fouquet, Y., and Normand, A., 2013, High-  
644 resolution bathymetry reveals contrasting landslide activity shaping the walls of  
645 the Mid-Atlantic Ridge axial valley: *GEOCHEMISTRY GEOPHYSICS*  
646 *GEOSYSTEMS*, v. 14, no. 4, p. 996–1011, doi: 10.1002/ggge.20056.
- 647 Cannat, M., Sauter, D., Lavier, L., Bickert, M., Momoh, E., and Leroy, S., 2019, On  
648 spreading modes and magma supply at slow and ultraslow mid-ocean ridges:  
649 *Earth and Planetary Science Letters*, v. 519, p. 223–233, doi:  
650 10.1016/j.epsl.2019.05.012.
- 651 Cheadle, M. J., John, B. E., German, C. R., & Kusznir, N. J., 2012, The death throes of  
652 ocean core complexes: Examples from the Mid-Cayman Spreading Centre.  
653 Abstract OS11E-01 Presented at 2012 Fall Meeting, AGU, San Francisco, Calif. 5-9  
654 Dec.
- 655 Cheadle, M. J., John, B. E., Schroeder, T. J., & Weber, M. L., 2019, Some things we've  
656 learned about oceanic core complexes, but we were afraid to ask. Abstract T12C-04  
657 Presented at 2019 Fall Meeting, AGU, San Francisco, Calif. 9-13 Dec.
- 658 Collins, J. a., Smith, D.K., and McGuire, J.J., 2012, Seismicity of the Atlantis Massif  
659 detachment fault, 30N at the Mid-Atlantic Ridge: *Geochemistry, Geophysics,*  
660 *Geosystems*, v. 13, no. 1, p. 1–14, doi: 10.1029/2012GC004210.
- 661 Cotterill, Carol; Früh-Green, Gretchen L (2021): Multibeam bathymetry processed data  
662 (Kongsberg EM 122 working area dataset) of RRS JAMES COOK during cruise  
663 IODP Expedition 357, Atlantis Massif. PANGAEA,  
664 <https://doi.org/10.1594/PANGAEA.935687>
- 665 Dick, H.J.B., Tivey, M.A., and Tucholke, B.E., 2008, Plutonic foundation of a slow-  
666 spreading ridge segment: Oceanic core complex at Kane Megamullion, 23° 30'N,  
667 45 °20'W: *Geochemistry, Geophysics, Geosystems*, v. 9, p. Q05014,  
668 doi:10.1029/2007GC001645.
- 669 De Martini, P.M., Pantosti, D., Palyvos, N., Lemeille, F., McNeill, L., and Collier, R.,  
670 2004, Slip rates of the Aigion and Eliki Faults from uplifted marine terraces,  
671 Corinth Gulf, Greece: *Comptes Rendus Geoscience*, v. 336, no. 4–5, p. 325–334,  
672 doi: 10.1016/j.crte.2003.12.006.
- 673 deMartin, B.J., Sohn, R.A., Canales, J.P., and Humphris, S.E., 2007, Kinematics and  
674 geometry of active detachment faulting beneath the Trans-Atlantic Geotraverse  
675 (TAG) hydrothermal field on the Mid-Atlantic Ridge: *Geology*, v. 35, no. 8, p. 711–  
676 714.
- 677 Escartín, J., Mével, C., MacLeod, C.J., and McCaig, A.M., 2003, Constraints on  
678 deformation conditions and the origin of oceanic detachments: The Mid-Atlantic  
679 Ridge core complex at 15°45'N: *Geochemistry, Geophysics, Geosystems*, v. 4, no.  
680 8, p. 1067, doi:10.1029/2001GC000278.



- Escartín, J., Mével, C., Petersen, S., Bonnemains, D., Cannat, M., Andreani, M., Augustin, N., Bezos, A., Chavagnac, V., Choi, Y., Godard, M., Haaga, K., Hamelin, C., Ildefonse, B., et al., 2017, Tectonic structure, evolution, and the nature of oceanic core complexes and their detachment fault zones (13°20'N and 13°30'N, Mid Atlantic Ridge): *Geochemistry, Geophysics, Geosystems*, v. 18, no. 4, p. 1451–1482, doi: 10.1002/2016GC006775.
- Escartín, J., Smith, D.K., Cann, J., Schouten, H., Langmuir, C.H., and Escrig, S., 2008, Central role of detachment faults in accretion of slow-spreading oceanic lithosphere: *Nature*, v. 455, no. 7214, p. 790–794, doi: 10.1038/nature07333.
- Früh-Green, G.L., Kelley, D.S., Bernasconi, S.M., Karson, J.A., Ludwig, K.A., Butterfield, D.A., Boschi, C., and Proskurowski, G., 2003, 30,000 Years of Hydrothermal Activity at the Lost City Vent Field: *Science*, v. 301, p. 495–498.
- Früh-Green, G.L., Orcutt, B.N., Green, S.L., Cotterill, C., Morgan, S., Akizawa, N., Bayrakci, G., Behrmann, J.-H., Boschi, C., Brazleton, W.J., Cannat, M., Dunkel, K.G., Escartín, J., Harris, M., Herrero-Bervera, E., Hesse, K., John, B.E., Lang, S.Q., Lilley, M.D., Liu, H.-Q., Mayhew, L.E., McCaig, A.M., Menez, B., Morono, Y., Quéméneur, M., Rouméjon, S., Sandaruwan Ratnayake, A., Schrenk, M.O., Schwarzenbach, E.M., Twing, K.I., Weis, D., Whattham, S.A., Williams, M., and Zhao, R., 2017, Expedition 357 summary, in Früh-Green, G.L., Orcutt, B.N., Green, S.L., Cotterill, C., and the Expedition 357 Scientists, *Atlantis Massif Serpentinization and Life. Proceedings of the International Ocean Discovery Program, 357: College Station, TX (International Ocean Discovery Program)*. <http://dx.doi.org/10.14379/iodp.proc.357.101.2017>.
- Früh-Green, G.L., Orcutt, B.N., Green, S.L., Cotterill, C., and the Expedition 357 Scientists, 2017. **Expedition 357 Methods**, <http://dx.doi.org/10.14379/iodp.proc.357supp.2017>. *Supplement to Früh-Green, G.L., Orcutt, B.N., Green, S.L., Cotterill, C., and the Expedition 357 Scientists, Atlantis Massif Serpentinization and Life. Proceedings of the International Ocean Discovery Program, 357: College Station, TX (International Ocean Discovery Program)*. <http://dx.doi.org/10.14379/iodp.proc.357.2017>.
- Früh-Green, G.L., Orcutt, B.N., Rouméjon, S., Lilley, M.D., Morono, Y., Cotterill, C., Green, S., Escartín, J., John, B.E., McCaig, A.M., Cannat, M., Menez, B., Schwarzenbach, E.M., Williams, M.J., et al., 2018, Magmatism, serpentinization and life: Insights through drilling the Atlantis Massif (IODP Expedition 357): *Lithos*, doi: 10.1016/j.lithos.2018.09.012.
- Fujiwara, T., Lin, J., Matsumoto, P.B., Tucholke, B., and Casey, J.F., 2003, Crustal evolution of the Mid-Atlantic Ridge near the Fifteen-Twenty Fracture Zone in the last 5 Ma: *Geochemistry, Geophysics, Geosystems*, v. 4, no. 3, p. 10.1029/2002GC000364.
- Garcés, M., and Gee, J.S., 2007, Paleomagnetic evidence of large footwall rotations associated with low-angle faults at the Mid-Atlantic Ridge: *Geology*, v. 35, no. 3, p. 279–282.
- Grimes, C.B., Cheadle, M.J., John, B.E., Reiners, P.W., and Wooden, J.L., 2011, Cooling

- 724 rates and the depth of detachment faulting at oceanic core complexes: Evidence  
725 from zircon Pb/U and (U-Th)/He ages: *Geochemistry, Geophysics, Geosystems*,  
726 v. 12, no. 3, p. n/a-n/a, doi: 10.1029/2010GC003391.
- 727 Grimes, C.B., John, B.E., Cheadle, M.J., and Wooden, J.L., 2008, Protracted construction  
728 of gabbroic crust at a slow spreading ridge: Constraints from <sup>206</sup>Pb/<sup>238</sup>U zircon  
729 ages from Atlantis Massif and IODP Hole U1309D (30°N, MAR): *Geochemistry*,  
730 *Geophysics, Geosystems*, v. 9, no. 8, p. Q08012, doi:10.1029/2008GC002063.
- 731 Hansen, L.N., Cheadle, M.J., John, B.E., Swapp, S.M., Dick, H.J.B., Tucholke, B.E., and  
732 Tivey, M. A., 2013, Mylonitic deformation at the Kane oceanic core complex:  
733 Implications for the rheological behavior of oceanic detachment faults:  
734 *Geochemistry, Geophysics, Geosystems*, v. 14, no. 8, p. n/a-n/a, doi:  
735 10.1002/ggge.20184.
- 736 Henig, A.S., Blackman, D.K., Harding, A.J., Canales, J.-P., and Kent, G.M., 2012,  
737 Downward continued multichannel seismic refraction analysis of Atlantis Massif  
738 oceanic core complex, 30°N, Mid-Atlantic Ridge: *Geochemistry Geophysics*  
739 *Geosystems*, v. 13, no. 1, p. Q0AG07, doi: 10.1029/2012GC004059.
- 740 Howell, S.M., Olive, J.-A., Ito, G., Behn, M.D., Escartín, J., and Kaus, B., 2019, Seafloor  
741 expression of oceanic detachment faulting reflects gradients in mid-ocean ridge  
742 magma supply: *Earth and Planetary Science Letters*, v. 516, p. 176–189, doi:  
743 10.1016/j.epsl.2019.04.001.
- 744 Ildefonse, B., Blackman, D.K., John, B.E., Ohara, Y., Miller, D.J., MacLeod, C.J., and  
745 Integrated IODP Expeditions Science Party, 2007, Oceanic core complexes and  
746 crustal accretion at slow-spreading ridges: *Geology*, v. 35, no. 7, p. 623–626.
- 747 John, B.E., and M. J. Cheadle, 2010, Deformation and alteration associated with oceanic  
748 and continental detachment fault systems: Are they similar?, *in* *Diversity of*  
749 *Hydrothermal Systems on Slow Spreading Ocean Ridges*, *Geophys. Monogr.*  
750 *Ser.*, vol.188, edited by P.A. Rona et al., pp.175–205, AGU, Washington, D.C.,  
751 doi:10.1029/2008GM000772.
- 752 Karson, J.A., Früh-Green, G.L., Kelley, D.S., Williams, E.A., Yoerger, D.R., and Jakuba,  
753 M., 2006, Detachment shear zone of the Atlantis Massif core complex, Mid-  
754 Atlantic Ridge, 30°N: *Geochemistry, Geophysics, Geosystems*, v. 7, no. 6, p.  
755 Q06016, doi:10.1029/2005GC001109.
- 756 Kelley, D.S., Karson, J.A., Früh-Green, G.L., Yoerger, D.R., Shank, T.M., Butterfield,  
757 D.A., Hayes, J.M., Schrenk, M.O., Olson, E.J., Proskurowski, G., Jakuba, M.,  
758 Bradley, A., Larson, B., Ludwig, K., et al., 2005, A Serpentinite-Hosted Ecosystem:  
759 The Lost City Hydrothermal Field: *Science*, v. 307, p. 1428–1434.
- 760 Lavier, L., Buck, W.R., and Poliakov, A.N.B., 1999, Self-consistent rolling-hinge model  
761 for the evolution of large-offset low-angle normal faults: *Geology*, v. 27, no. 12, p.  
762 1127–1130.

- 763 Lavier, L., Buck, W.R., and Poliakov, A.N.B., 2000, Factors controlling normal fault  
764 offset in an ideal brittle layer: *Journal of Geophysical Research*, v. 105, no. B10, p.  
765 23431–23442.
- 766 MacLeod, C.J., Carlut, J., Escartín, J., Horen, H., and Morris, A., 2012, Quantitative  
767 constraint on footwall rotations at the 1545N oceanic core complex, Mid-Atlantic  
768 Ridge: Implications for oceanic detachment fault processes: *Geochemistry,*  
769 *Geophysics, Geosystems*, v. 12, no. 5, doi: 10.1029/2011GC003503.
- 770 MacLeod, C.J., Searle, R.C., Casey, J.F., Mallows, C., Unsworth, M., Achenbach, K., and  
771 Harris, M., 2009, Life cycle of oceanic core complexes: *Earth and Planetary Science*  
772 *Letters*, v. 287, p. 333–344.
- 773 Mallows, C., and Searle, R.C., 2012, A geophysical study of oceanic core complexes  
774 and surrounding terrain, Mid-Atlantic Ridge 13°N–14°N: *Geochemistry*  
775 *Geophysics Geosystems*, v. 13, no. 1, p. Q0AG08, doi: 10.1029/2012GC004075.
- 776 Morris, A.R., Gee, J.S., Pressling, N.J., John, B.E., MacLeod, C.J., Grimes, C.B., and  
777 Searle, R.C., 2009, Footwall rotation in an oceanic core complex quantified using  
778 reoriented Integrated Ocean Drilling Program core samples: *Earth and Planetary*  
779 *Science Letters*, v. 287, p. 217–228.
- 780 Ohara, Y., 2016, The Godzilla Megamullion, the largest oceanic core complex on the  
781 earth: a historical review: *Island Arc*, v. 25, no. 3, p. 193–208, doi:  
782 10.1111/iar.12116.
- 783 Okino, K., Matsuda, K., Christie, D.M., Nogi, Y., and Koizumi, K., 2004, Development  
784 of oceanic detachment and asymmetric spreading at the Australian-Antarctic  
785 Discordance: *Geochemistry, Geophysics, Geosystems*, v. 5, no. 12, p. Q12012,  
786 doi:10.1029/2004GC000793.
- 787 Olive, J.-A., Behn, M.D., Mittelstaedt, E., Ito, G., and Klein, B.Z., 2016, The role of  
788 elasticity in simulating long-term tectonic extension: *Geophysical Journal*  
789 *International*, v. 205, no. 2, p. 728–743, doi: 10.1093/gji/ggw044.
- 790 Olive, J. A., M. D. Behn, and B. E. Tucholke (2010), The structure of oceanic core  
791 complexes controlled by the depth distribution of magma emplacement, *Nat.*  
792 *Geosci.*, 3, 491–495, doi:10.1038/ngeo888.
- 793 Olive, J.-A., Parnell-Turner, R., Escartín, J., Smith, D.K., and Petersen, S., 2019,  
794 Controls on the seafloor exposure of detachment fault surfaces: *Earth and*  
795 *Planetary Science Letters*, v. 506, p. 381–387, doi: 10.1016/j.epsl.2018.11.001.
- 796 Pariso, J.E., Sempéré, J.-C., and Rommeveaux, C., 1995, Temporal and spatial  
797 variations in crustal accretion along the Mid-Atlantic Ridge (29° - 31°31'N) over  
798 the last 10 Ma: Implications from a three-dimensional gravity study: *Journal of*  
799 *Geophysical Research*, v. 100, no. 9, p. 17781–17794.

- 800 Parnell-Turner, R., Sohn, R.A., Peirce, C., Reston, T.J., MacLeod, C.J., Searle, R.C., and  
801 Simão, N.M., 2017, Oceanic detachment faults generate compression in extension:  
802 *Geology*, v. 45, no. 10, p. 923–926, doi: 10.1130/G39232.1.
- 803 Parnell-Turner, R., Escartín, J., Olive, J.-A., Smith, D.K., and Petersen, S., 2018, Genesis  
804 of corrugated fault surfaces by strain localization recorded at oceanic  
805 detachments: *Earth and Planetary Science Letters*, v. 498, p. 116–128, doi:  
806 10.1016/j.epsl.2018.06.034.
- 807 Proskurowski, G., Lilley, M. D., Seewald, J. S., Früh-Green, G. L., Olson, E. J., Lupton,  
808 J. E., Sylva, S. P., & Kelley, D. S. (2008). Abiogenic hydrocarbon production at Lost  
809 City hydrothermal field. *Science*, 319(5863), 604–607
- 810 Reston, T., 2018, Flipping detachments: The kinematics of ultraslow spreading ridges:  
811 *Earth and Planetary Science Letters*, v. 503, p. 144–157, doi:  
812 10.1016/j.epsl.2018.09.032.
- 813 Reston, T.J., Weinrebe, W., Grevemeyer, I., Flueh, N.C., Kirstein, L., Kopp, C., Kopp,  
814 H., and Participants, M. 47/2, 2002, A rifted inside corner massif on the Mid-  
815 Atlantic Ridge at 5°S: *Earth and Planetary Science Letters*, v. 200, p. 255–269.
- 816 Ryan, W.B.F., Carbotte, S.M., Coplan, J.O., O'Hara, S., Melkonian, A., Arko, R.,  
817 Weissel, R.A., Ferrini, V., Goodwillie, A., Nitsche, F., Bonczkowski, J., and  
818 Zemsky, R., 2009, Global Multi-Resolution Topography synthesis: *Geochemistry,*  
819 *Geophysics, Geosystems*, v. 10, no. 3, p. n/a-n/a, doi: 10.1029/2008GC002332.
- 820 Sandiford, D., Brune, S., Glerum, A., Naliboff, J., and Whittaker, J.M., 2021,  
821 Kinematics of Footwall Exhumation at Oceanic Detachment faults: Solid-Block  
822 Rotation and Apparent Unbending: *Geochemistry, Geophysics, Geosystems*, v.  
823 22, no. 4, p. 1–12, doi: 10.1029/2021GC009681.
- 824 Sauter, D., Cannat, M., Rouméjon, S., Andreani, M., Birot, D., Bronner, A., Brunelli, D.,  
825 Carlut, J., Delacour, A., Guyader, V., MacLeod, C.J., Manatschal, G., Mendel, V.,  
826 Ménez, B., et al., 2013, Continuous exhumation of mantle-derived rocks at the  
827 Southwest Indian Ridge for 11 million years: *Nature Geoscience*, v. 6, no. 4, p.  
828 314–320, doi: 10.1038/ngeo1771.
- 829 Schoolmeesters, N., Cheadle, M.J., John, B.E., Reiners, P.W., Gee, J., and Grimes, C.B.,  
830 2012, The cooling history and the depth of detachment faulting at the Atlantis  
831 Massif oceanic core complex: *Geochemistry Geophysics Geosystems*, v. 13, no. 1,  
832 p. 1–19, doi: 10.1029/2012GC004314.
- 833 Schouten, H., Smith, D.K., Cann, J.R., and Escartín, J., 2010, Tectonic versus magmatic  
834 extension in the presence of core complexes at slow-spreading ridges from a  
835 visualization of faulted seafloor topography: *Geology*, v. 38, no. 7, doi:  
836 10.1130/G30803.1.
- 837 Schroeder, T., and B. E. John, 2004, Strain localization on an oceanic detachment fault  
838 system, Atlantis Massif, 30°N, Mid-Atlantic Ridge, *Geochem. Geophys. Geosyst.*,  
839 5, Q11007, doi:10.1029/2004GC000728.

- 840 Searle, R.C., Cannat, M., Fujioka, K., Mével, C., Fujimoto, H., Bralee, A., and Parson,  
841 L., 2003, FUJI Dome: A large detachment fault near 64 E on the very slow-  
842 spreading southwest Indian Ridge: *Geochemistry, Geophysics, Geosystems*, v. 4,  
843 no. 8, p. 9105, doi:10.1029/2003GC000519.
- 844 Seyfried, W.E., Pester, N.J., Tutolo, B.M., and Ding, K., 2015, The Lost City  
845 hydrothermal system: Constraints imposed by vent fluid chemistry and reaction  
846 path models on subseafloor heat and mass transfer processes: *Geochimica et*  
847 *Cosmochimica Acta*, v. 163, p. 59–79, doi: 10.1016/j.gca.2015.04.040.
- 848 Smith, D.K., Escartín, J., Schouten, H., and Cann, J.R., 2008, Fault rotation and core  
849 complex formation: Significant processes in seafloor formation at slow-spreading  
850 mid-ocean ridges (Mid-Atlantic Ridge, 13 –15° N): *Geochemistry, Geophysics,*  
851 *Geosystems*, v. 9, no. 3, p. Q03003, doi:10.1029/2007GC001699.
- 852 Smith, D.K., Tivey, M.A., Schouten, H., and Cann, J.R., 1999, Locating the spreading  
853 axis along 80 km of the Mid-Atlantic Ridge south of the Atlantis Transform:  
854 *Journal of Geophysical Research*, v. 104, p. 7599–7612.
- 855 Tani, K., D. J. Dunkley, and Y. Ohara (2011), Termination of backarc spreading: Zircon  
856 dating of a giant oceanic core complex, *Geology*, 39, 47–50.
- 857 Thibaud, R., Gente, P., and Maia, M., 1998, A systematic analysis of the Mid-Atlantic  
858 Ridge morphology between 15°N and 40°N: Constraints of the thermal structure:  
859 *Journal of Geophysical Research*, v. 103, no. B10, p. 24233–24243.
- 860 Tucholke, B.E., Behn, M.D., Buck, W.R., and Lin, J., 2008, Role of melt supply in oceanic  
861 detachment faulting and formation of megamullions: *Geology*, v. 36, no. 6, p. 455–  
862 458; doi: 10.1130/G24639A.
- 863 Tucholke, B.E., Lin, J., and Kleinrock, M.C., 1998, Megamullions and mullion structure  
864 defining oceanic metamorphic core complexes on the Mid-Atlantic ridge: *J*  
865 *Geophysical Research*, 103, B5, 9857–9866.
- 866 Webber, S., Norton, K.P., Little, T.A., Wallace, L.M., and Ellis, S., 2018, How fast can  
867 low-angle normal faults slip? Insights from cosmogenic exposure dating of the  
868 active Mai'iu fault, Papua New Guinea: *Geology*, v. 46, no. 3, p. 227–230, doi:  
869 10.1130/G39736.1.
- 870 Xu, M., J. P. Canales, B. E. Tucholke, and D. L. DuBois (2009), Heterogeneous seismic  
871 velocity structure of the upper lithosphere at Kane oceanic core complex, Mid-  
872 Atlantic Ridge; *Geochem. Geophys. Geosyst.*, 10, Q10001, doi:10.1029/  
873 2009GC002586.
- 874 Yeo, I., Searle, R.C., Achenbach, K.L., Le Bas, T.P., and Murton, B.J., 2011, Eruptive  
875 hummocks: Building blocks of the upper ocean crust: *Geology*, v. 40, no. 1, p. 91–  
876 94, doi: 10.1130/G31892.1.
- 877 Zervas, C.E., Sempéré, J.C., and Lin, J., 1995, Morphology and crustal structure of a  
878 small transform fault along the Mid-Atlantic Ridge: The Atlantis Fracture Zone:  
879 *Marine Geophysical Researches*, v. 17, no. 3, p. 275–300, doi: 10.1007/BF01203466.

880

## Figures

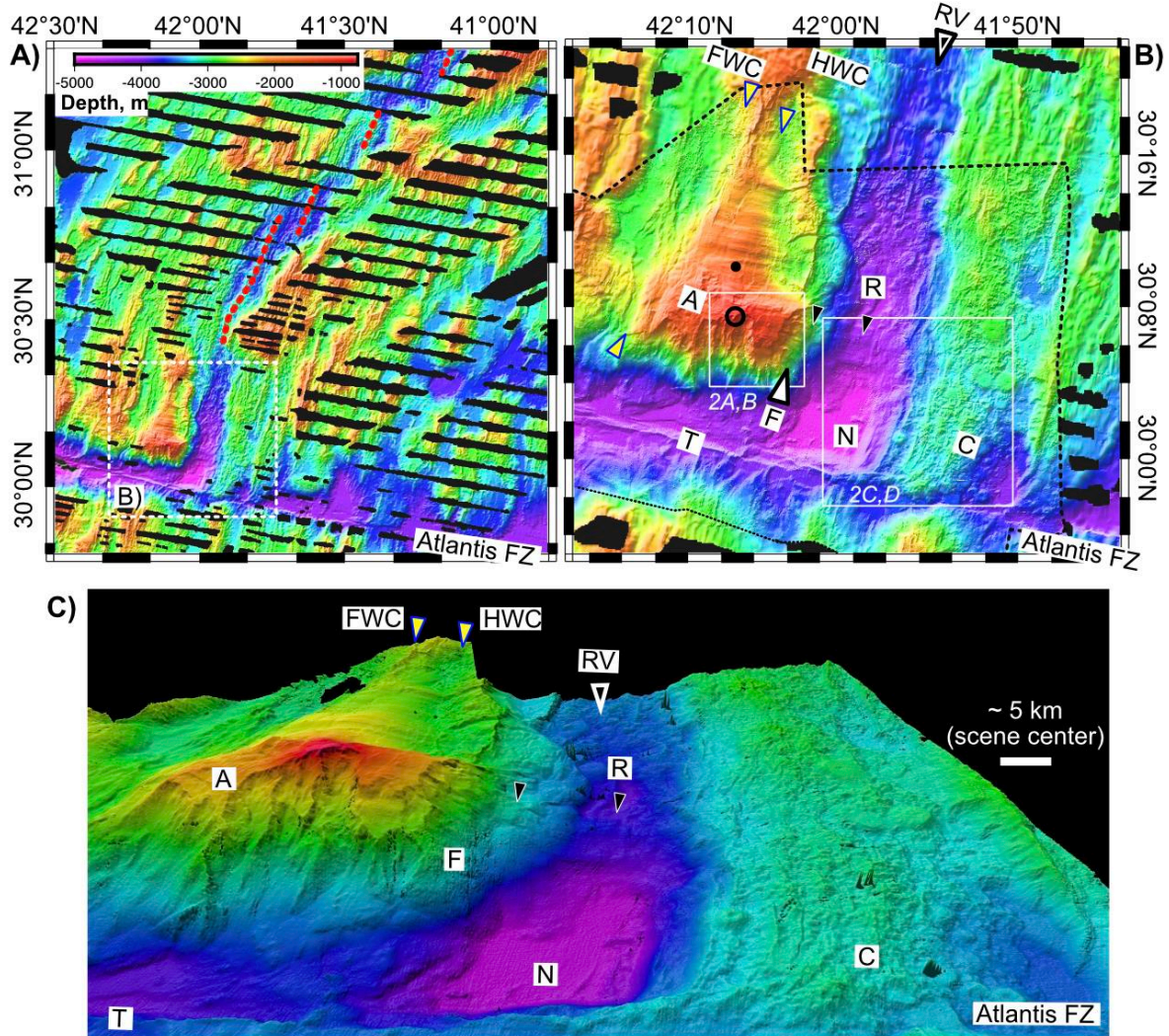


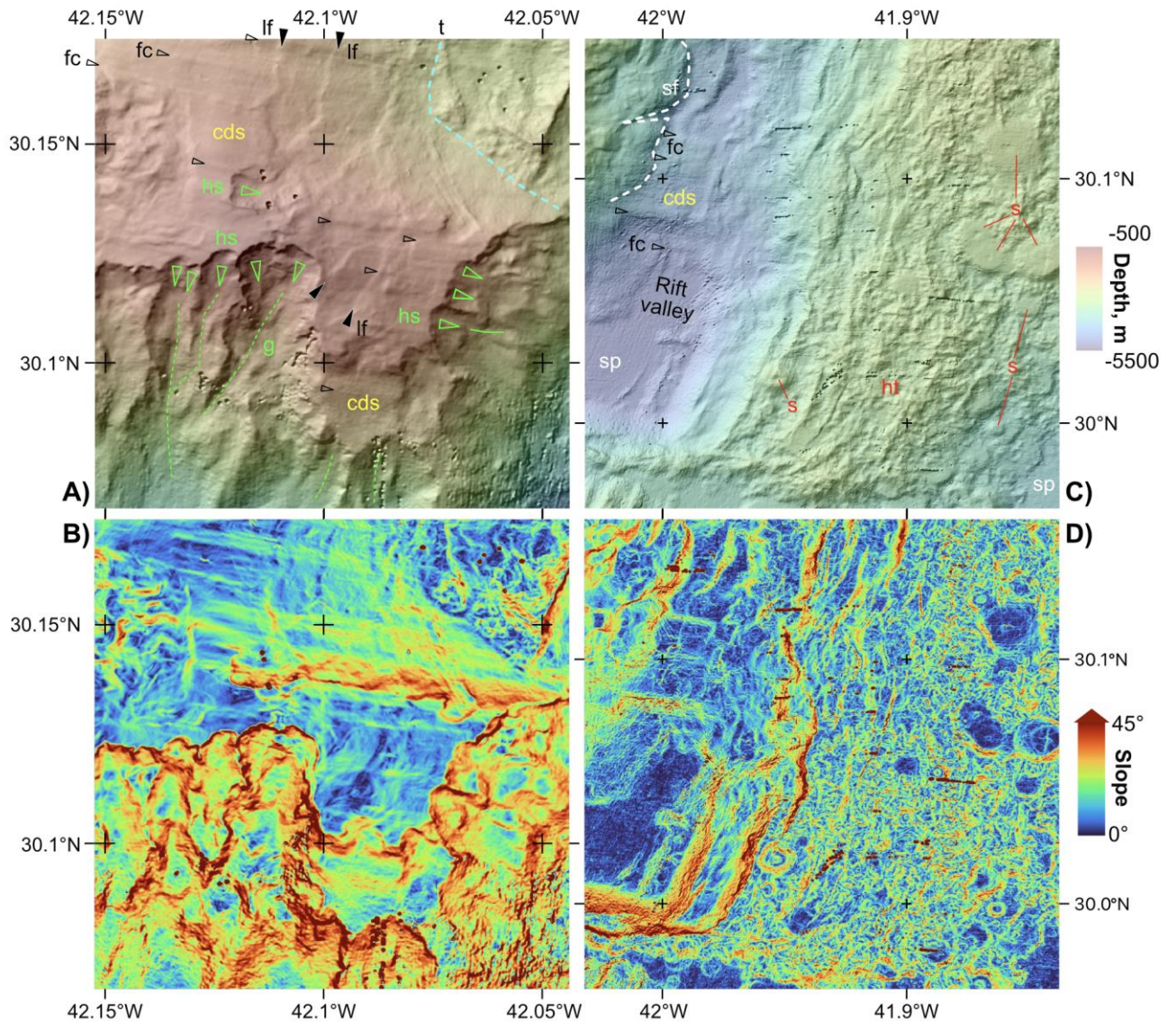
**Figure 1.** A) Regional bathymetric map of the Mid-Atlantic Ridge at 30° N, showing the location of the study area and the regional ridge geometry and segmentation; axial volcanic ridges indicated by red dashed lines. Dashed white box outlines location of B). B) Bathymetry of the Atlantis Massif detachment, adjacent ridge axis, and conjugate flank. Dashed black is the limit of the multibeam bathymetry survey acquired during cruise JC130 onboard RRS James Cook, gridded at 20 m, and complemented with open-access data available at [www.gmrt.org](http://www.gmrt.org) (Ryan et al., 2009). This bathymetry grid is publicly available (<https://doi.pangaea.de/10.1594/PANGAEA.935687>). C) Perspective view of the rift valley, the Atlantis Detachment system, and the conjugate crust showing volcanic seafloor. Labels in B)



and C): Atlantis detachment system (A); Conjugate flank with volcanic seafloor from paleo-roft valley; Open triangles: axis of the rift valley (RV); yellow-filled triangles: hanging wall and footwall cutoffs (HWC and FWC respectively); white-filled triangle: western rift bounding fault dissecting the southern part of the detachment (F); The rift valley shows a deep nodal basin (N) adjacent to the Atlantis transform fault (T), as well as remnants of the detachment fault (R), indicated by small black triangles. Open circle: Lost City hydrothermal field; black circle: IODP Hole U1309D. Supplementary Figure S1 provides detailed bathymetry (Figure S1A), shaded relief (Figure S1B), and slope maps (Figure S1C). White boxes in B locate panels in Figure 2.



904

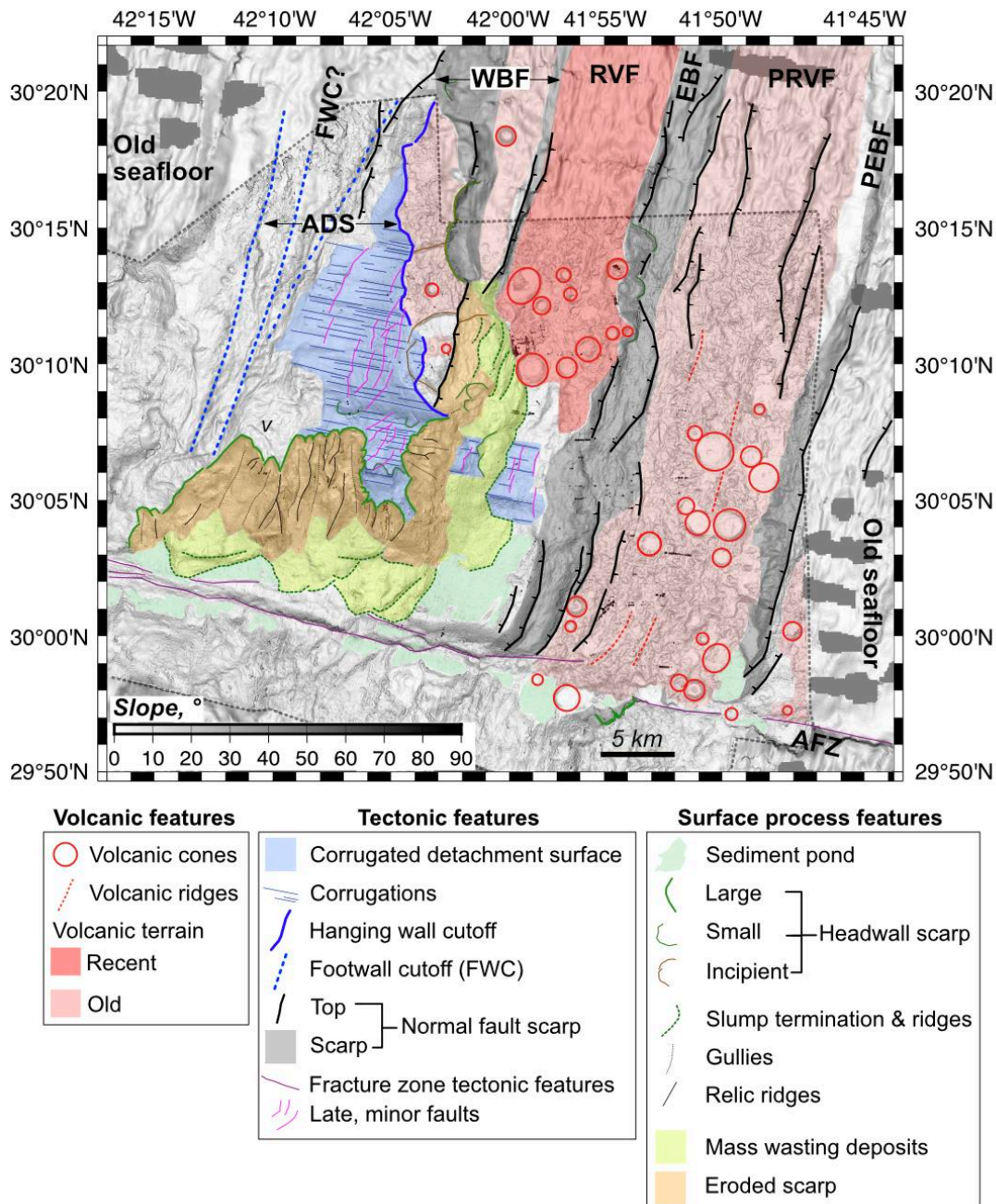


905

906 **Figure 2.** Detailed bathymetric maps highlighting selected seafloor geomorphic features. A)  
 907 Bathymetry of the Atlantis Massif southern summit, with the corrugated detachment fault  
 908 surface (cds), with clear extension-parallel corrugations (fc, open black triangles) late small-  
 909 scale faults cross-cutting the corrugations (lf, black solid triangles), and the detachment  
 910 termination (t), or hanging wall cutoff. The transform wall (south) and rift valley wall (East)  
 911 show mass wasting structures with curved head scarps (hs, green open triangles), and gullies  
 912 (g, green open triangles) separated by ridges. B) Slope map of the area shown in A). C)  
 913 Southern end of the present-day rift valley, bound by the Atlantis Fracture Zone, showing the  
 914 remnants of the corrugated detachment (cds) and associated corrugations (fc). The southern



915 end of the rift valley corresponds to a flat-bottomed sediment pond (sd). The seafloor on the East  
 916 flank shows hummocky terrain (ht) peppered by seamounts (s).



917

918 **Figure 3.** Geomorphologic interpretation of Atlantis Massif, showing features associated with  
 919 volcanic, tectonic, and surface processes, on bathymetric slope map. The figure highlights the  
 920 present-day rift valley floor (RVF), its West and East bounding faults (WBF and EBF,  
 921 respectively), the interpreted paleo-rift valley floor (PRVF), its paleo-East bounding fault  
 922 (PEBF), the Atlantis detachment system (ADS) limited to the West by possible footwall cutoffs  
 923 (FWC?), and the Atlantis Fracture Zone (AFZ) to the South. Also shown is the location of

young and glassy volcanic rocks erupted onto the detachment (v), from shallow core descriptions recovered from IODP Expedition 357 (Früh-Green, et al, 2017).

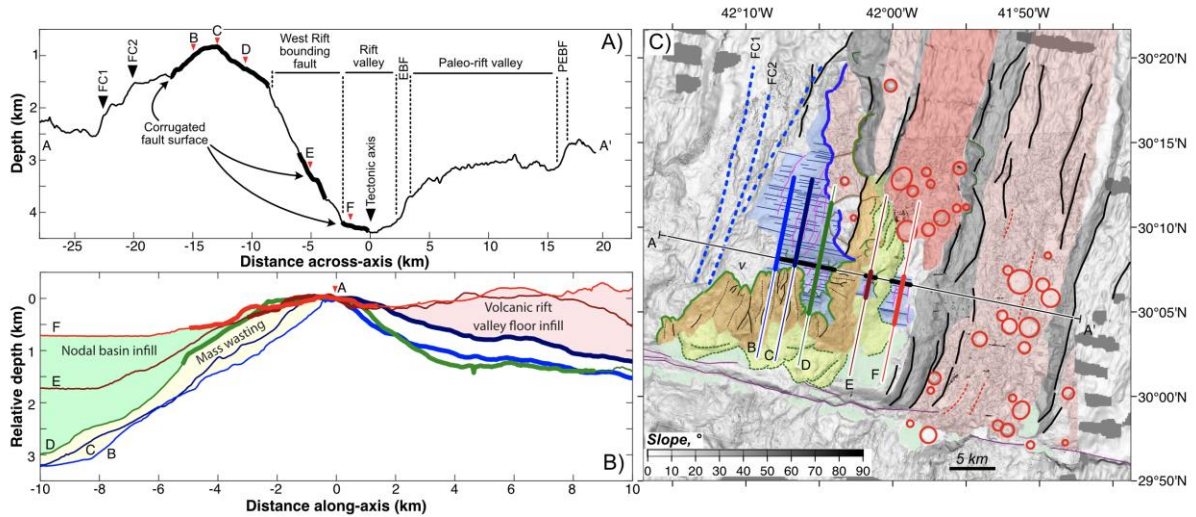


**Figure 4.** Across- and along-axis bathymetric profiles over the Atlantis Massif detachment system. Profile location (A through F) shown on C). A) Profile A-A' crosses two preserved portions of the corrugated fault surface along the rift bounding fault and floor (bold line). The tectonic axis (0 km) is assigned as the eastern limit of the detachment surface at the rift floor. Intersections of section A-A' by ridge-parallel profiles in B) shown as red triangles and associated letters (see location in C). FC: Footwall cutoff; EBF and PEBF: East boundary fault and paleo east boundary fault. B) Along-axis profiles over the two remnants of the detachment floor at the rift valley floor (F), and wall (E) and extending towards the flat-bottomed southern nodal basin, and over the main detachment surface (profiles B through D). All profiles are shifted vertically and stacked with a depth of 0 km at the crossing with profile A, to obtain a relative structural depth below the detachment fault surface. Portions of profiles across the detachment fault surface are bold. Differences in relative depth between profiles F and C to the North correspond to the volcanic infill of the rift valley floor; in the south, to the nodal basin infill. Differences between profiles B and C and profile D (to the south) corresponds to the mass-wasted footwall talus on the transform valley wall. See text for detailed discussion.

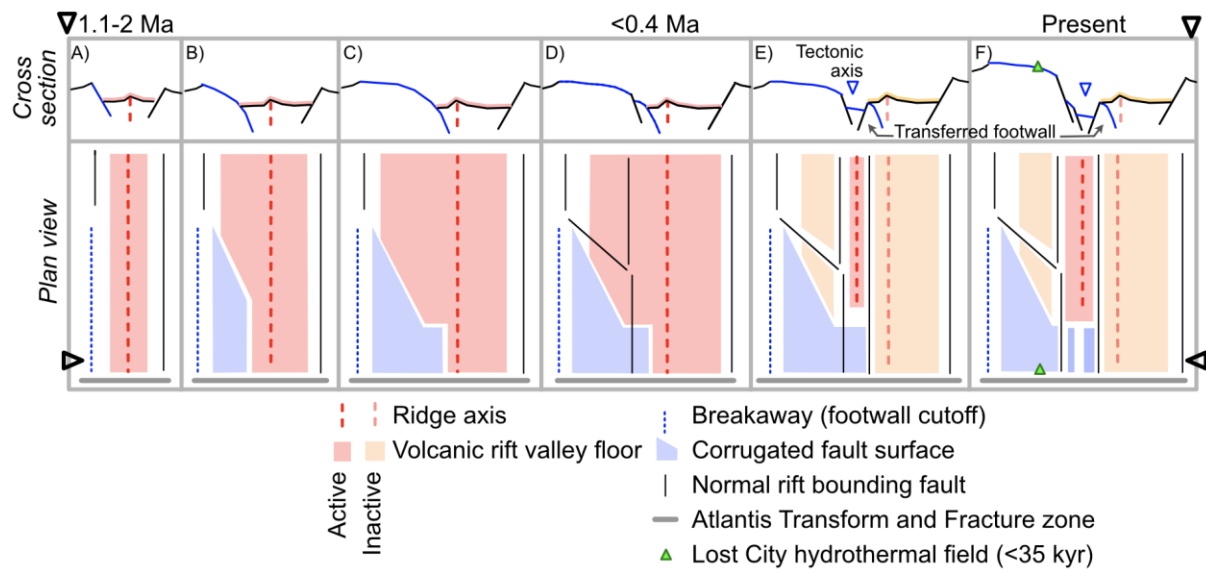
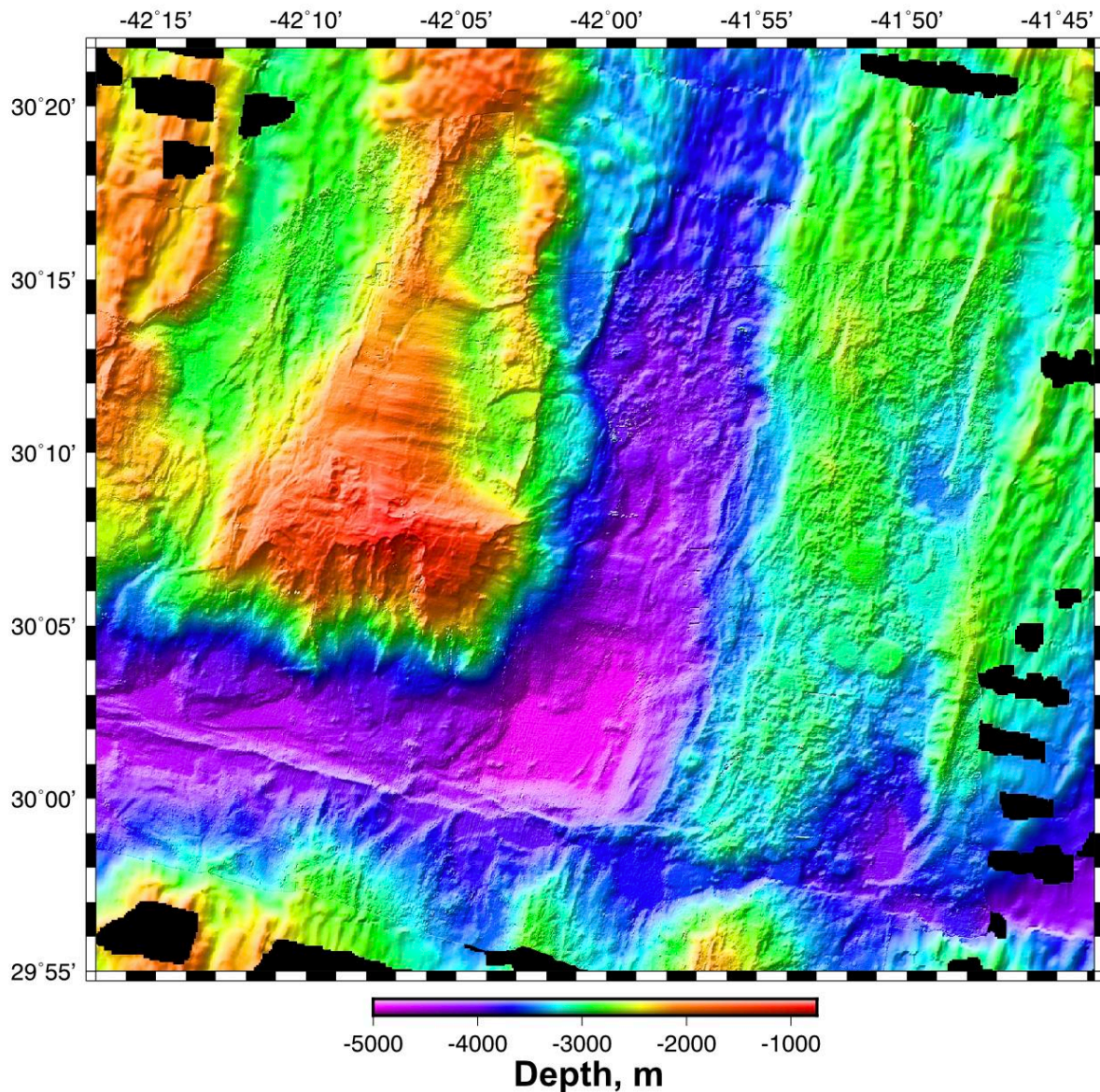


Figure 5. Schematic tectonic history of the Atlantis Massif detachment system. Top panels show a cross-section at the southern part of the detachment system. The bottom panels are a simplified plan view of the tectonic evolution illustrating the along-axis variations in tectonic and volcanic processes, with the open black triangles indicating the position of the across axis profile on the upper panels. The system initiated ~1.1-2 Ma ago (A), with a detachment that shortened along-axis towards the transform fault, where it is best developed (B and C). (D) A newly formed rift bounding fault dissects both the tip of the detachment and the volcanic seafloor to the north of it on the west flank, ~0.4 Ma ago or earlier. This new fault is associated with the formation of a new rift valley, paved with volcanics to the North, and remnants of the detachment surface to the south. Part of the detachment footwall is also transferred to the East flank across the newly formed tectonic axis (E). With continued extension the paleo-rift valley floor is rafted off-axis while the present-day axial graben develops. Detachment remnants, while dissected by faults, pave the rift valley floor and document avolcanic extension (F). Emplacement of the Lost City hydrothermal system occurred <35 kyrs (Fruh-Green et al., 2003), during the latest stage and post-dating the avolcanic rift valley formation (F).

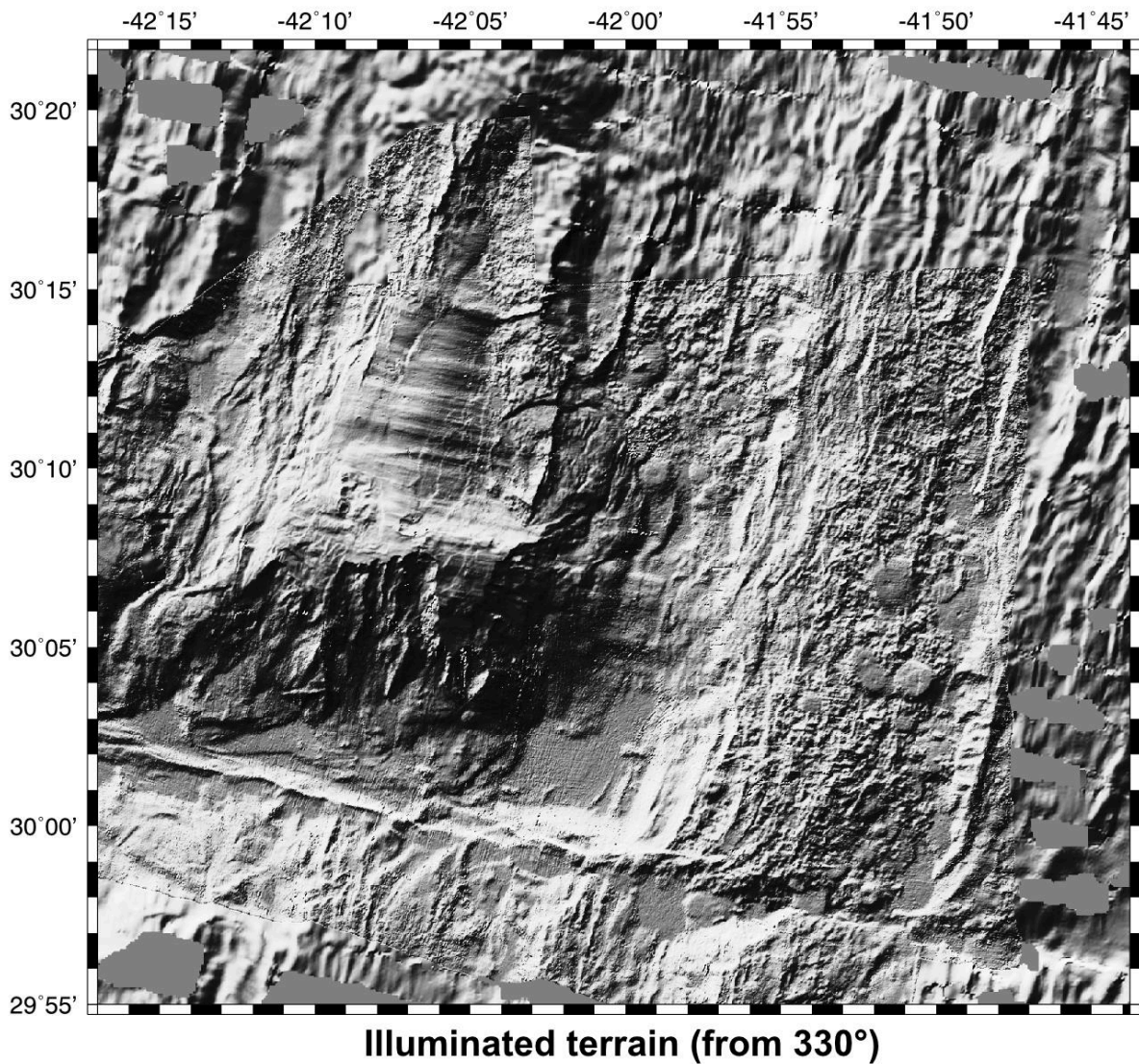


## Supplementary Materials



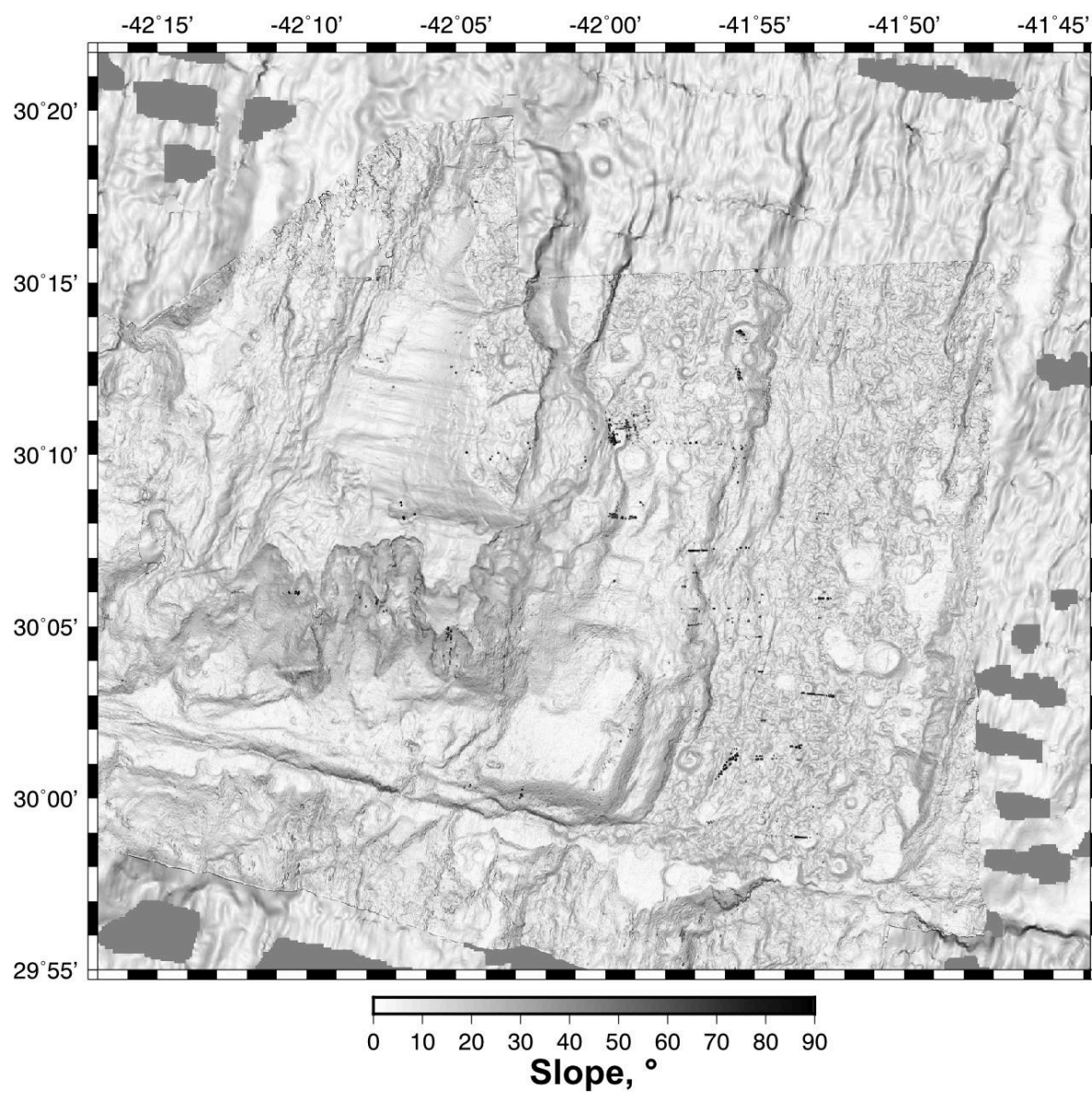
**Supplementary Figure 1.** A) Shaded relief bathymetric map of the study area, combining moderate- high-resolution data from the IODP 357 Expedition survey (Früh-Green *et al.*, 2018), with earlier data from the MARVEL 2000 cruise (Blackman *et al.*, 2002), and other publicly available data through the Global Multi-Resolution Topography Data Synthesis at [www.gmrt.org](http://www.gmrt.org) (Ryan *et al.*, 2009). Data gridded at 20 m resolution. Although this high-resolution gridding does not filter some of the bathymetry processing artifacts and noise, it reveals fine-scale structures associated with volcanic, tectonic, and mass wasting processes. B) Shaded relief (no depth-

976 colour mapping) of the same data shown in A). C) Seafloor slope from the same data  
977 shown in A).



978

979 **Supplementary Figure 1B.**



980

981 **Supplementary Figure 1C.**

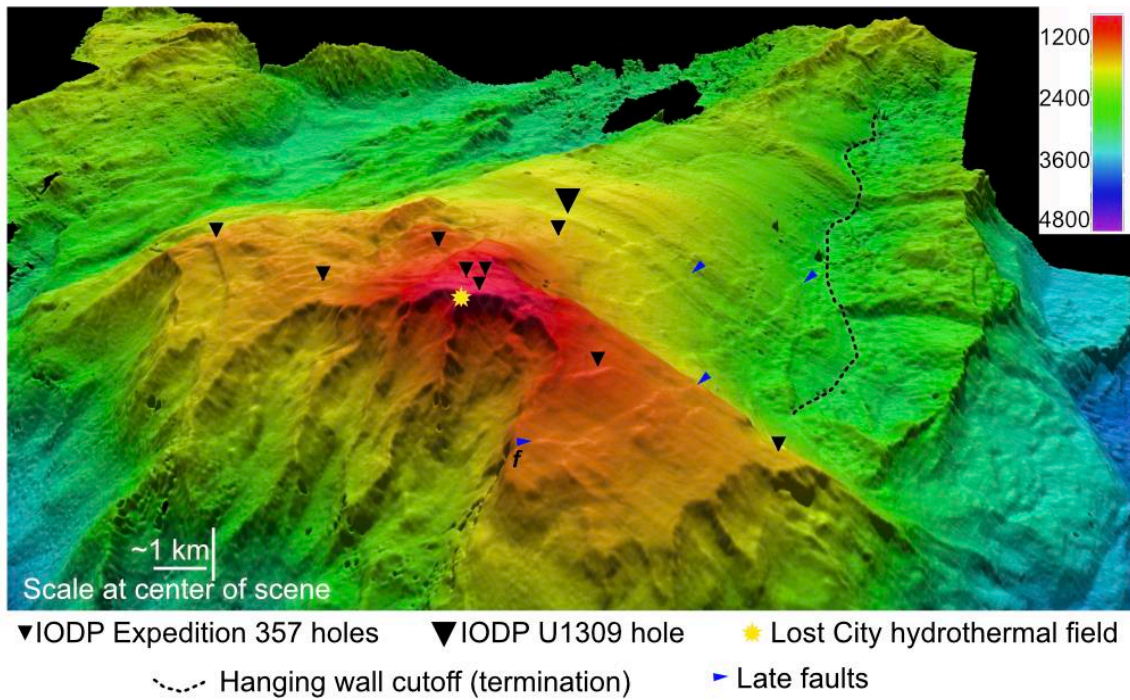
982

983

984



985



986

987 **Supplementary Figure 3.** Oblique three-dimensional view of the Atlantis Massif,  
 988 looking NNW. The rift axis is located to the right of the figure, and the Atlantis  
 989 Fracture zone at the base of the scarp in the foreground showing mass-wasting  
 990 scarps and the Lost City hydrothermal field. The view also shows the location of  
 991 IODP holes drilled during Expedition 357, and the position of the 1.5 km deep IODP  
 992 Hole U1309D, for reference.